

D. 11.2.1 Site specific report on geophysical survey on Teesside site (UK)

Jean-Christophe GOURRY¹ , Marc DUMONT²,

^{1.} BRGM,

^{2.} University of Liège



SUMMARY

1	Introduction.....	4
2	Teesside site description.....	4
2.1	Situation.....	4
2.2	Topography	7
2.2.1	DEM from GPS data	8
2.2.2	DEM from photogrammetry.....	9
2.3	Geological settings and site description	10
3	Geophysical survey.....	12
3.1	Geomagnetic survey	12
3.1.1	Survey strategy and data processing	12
3.1.2	Results	14
3.2	Electromagnetic (EMI) survey	17
3.2.1	Survey strategy and data processing	17
3.2.2	Results	19
3.3	Electrical resistivity and Induced Polarization tomography survey.....	22
3.3.1	Survey strategy and data processing	22
3.3.2	ERT/IP processing.....	25
3.3.3	ERT Results	34
4	Synthesis and discussion.....	35
4.1	Synthesis of results.....	35
4.2	Borehole localization.....	35
5	Conclusions	37
6	References	38

LIST OF FIGURES

Figure 1 : General views of Teesside site, a. general traffic view (Google Maps), b. and c. Google Earth views at different scales. The red line surrounds the experimental area.....	5
Figure 2 : Aerial view obtained with unmanned aerial vehicle (UAV) over the Teesside experimental site.....	6
Figure 3 : Aerial photos from Teesside area.....	7
Figure 4 : Topography of Teesside site evaluated from GPS data	8
Figure 5 : DEM obtained from UAV photogrammetry	9
Figure 6 : Elevation difference map between UAV DEM and GPS DEM	10
Figure 7 : Geological map of Teesside site (British Geological Survey 1/50000 map, Guisborough). The test site is surrounded by a dashed red line	11
Figure 8 : Geological schematic cross-section of the survey area. The left vertical scale is the AOD (or OD) reference. The right vertical scale is the ASL reference.....	11
Figure 9 : Geophysics crew on Teesside field. A. from left to right : Tutu Sebastian, Niall Marsay, Stuart Higson, Jean-Christophe Gourry and Alison Colombain. B. from left to right : Tutu Sebastian, Niall Marsay, Stuart Higson, Marc Dumont and Alison Colombain.	12
Figure 10 : Magnetic field measurements points map with Geometrics G858 magnetometer.....	13
Figure 11 : Magnetic susceptibility measurement points with the Bartington MS2D kappameter... ..	14
Figure 12 : Magnetic field gradient map	15
Figure 13 : Magnetic susceptibility measurement map (logarithmic scale)	16
Figure 14 : Correlation graph between surficial magnetic susceptibility and magnetic field gradient.	16
Figure 15 : photography of the DUALEM421S tool on Teesside site.....	17
Figure 16 : Schematic details of the DUALEM421S tool.....	18
Figure 17 : DUALEM421S survey measurement points	19
Figure 18 : Histogram of EMI data from the raw data, after outliers withdrawal and resampling. ...	20
Figure 19 : Scatter plot of EMI dataset with raw data (red dots), without outliers (blue dots), and resampled dataset (green dots). This plots allow to see the value of removed dataset.	21
Figure 20 : Ground electrical conductivity from HCP coils.	21
Figure 21 : Ground electrical conductivity from PRP coils.	22
Figure 22 : Position of the 5 ERT profiles on Teesside site	23
Figure 23 : Photo of the Syscal Terra equipment used for the Electrical Resistivity and IP Tomography survey	24
Figure 24 : Photographies of the ERT equipment on the Teesside site, in a vegetated area (left) and on a coarse-grained material (right)	24
Figure 25 : Electrical resistivity (top) and chargeability (bottom) models obtained in ERT1. Both profiles are blanked below the sensitivity limit. pyBERT inversion results	26
Figure 26 : Electrical resistivity (top) and chargeability (bottom) models obtained in ERT2. Both profiles are blanked below the sensitivity limit. In this profile, data around 100 m of distance have	

been biases during the acquisition. The resistivity and chargeability obtain between 80 and 120 m of distance came from the interpolation of surrounding values. The high chargeability anomaly should be considered as an artefact. . pyBERT inversion results 26

Figure 27 : Electrical resistivity (top) and chargeability (bottom) models obtained in ERT3. Both profiles are blanked below the sensitivity limit. pyBERT inversion results 27

Figure 28 : Electrical resistivity (top) and chargeability (bottom) models obtained in ERT4. Both profiles are blanked below the sensitivity limit. pyBERT inversion results 27

Figure 29 : Electrical resistivity (top) and chargeability (bottom) models obtained in ERT5. Both profiles are blanked below the sensitivity limit. pyBERT inversion results 28

Figure 30 : 3D view of the 5 resistivity profiles covered by the digital surface model. 28

Figure 31 : 3D view of the 5 chargeability profiles covered by the digital surface model..... 29

Figure 32 : ERT1.tomography. Top : Electrical resistivity cross-section, middle : Chargeability cross-section, bottom: Metal Factor cross-section. Dash black line represents the mean elevation of the heap bottom. Res2Inv inversion results. 30

Figure 33 : ERT2.tomography. Top : Electrical resistivity cross-section, middle : Chargeability cross-section, bottom: Metal Factor cross-section. Dash black line represents the mean elevation of the heap bottom. Res2Inv inversion results. 31

Figure 34 : ERT3 .tomography. Top : Electrical resistivity cross-section, middle : Chargeability cross-section, bottom: Metal Factor cross-section. Dash black line represents the mean elevation of the heap bottom. Res2Inv inversion results. 32

Figure 35 : ERT4.tomography. Top : Electrical resistivity cross-section, middle : Chargeability cross-section, bottom: Metal Factor cross-section. Dash black line represents the mean elevation of the heap bottom. Res2Inv inversion results. 33

Figure 36 : ERT5.tomography. Top : Electrical resistivity cross-section, middle : Chargeability cross-section, bottom: Metal Factor cross-section. Dash black line represents the mean elevation of the heap bottom. Res2Inv inversion results. 34

Figure 37 : Position of the 5 boreholes proposed for control 37

LIST OF TABLES

Table 1 : Table of coordinates of the 5 boreholes for control..... 36

1 INTRODUCTION

Teesside site is one of the three pilot sites of the NWE-REGENERATIS project. It is a former tailing pond owned by the TEESWORKS Limited in charge of the remediation, rehabilitation and redevelopment of the former industrial Megasite. The experimental site, called CLE31, has been identified by Material Processing institute (MPI) in collaboration with TEESWORKS authorities. The site has been chosen for two main reasons: (1) it hosted various activities for iron based alloys production; (2) it was just rehabilitated on surface, and historic documentation and investigations are done with respect of the UK legislation and threshold values. One of the interests of this site is that it allows testing the REGENERATIS methodologies developed within WPT1 and WPT2 on a site that has already been remediated.

The following report describes the site-geophysical survey on Teesside site that will be used for: (1) the creation of the geophysical database needed to design the SMARTIX (WP T2- A4) and (2) the performance reports on the Geophysical Characterization Method (WP T3- A1). The survey aims at classifying and identifying different kind of wastes in a heap of metallurgical wastes.

2 TEESSIDE SITE DESCRIPTION

2.1 SITUATION

The site is situated along the road from Middlesbrough to Redcar (North Yorkshire, UK), on southern bank of the Tees River., and is located close to the shoreline (Figure 1). The heap has a triangle shape with a 10 hectares surface, and is 10 to 12 m high around (Figure 2).

Aerial views obtained with an unmanned aerial vehicle (UAV) (Figure 3) show that the soil is mainly nude, covered with slags. A poor vegetation composed of short grass has grown sparsely except at the northern part with a dense bush.

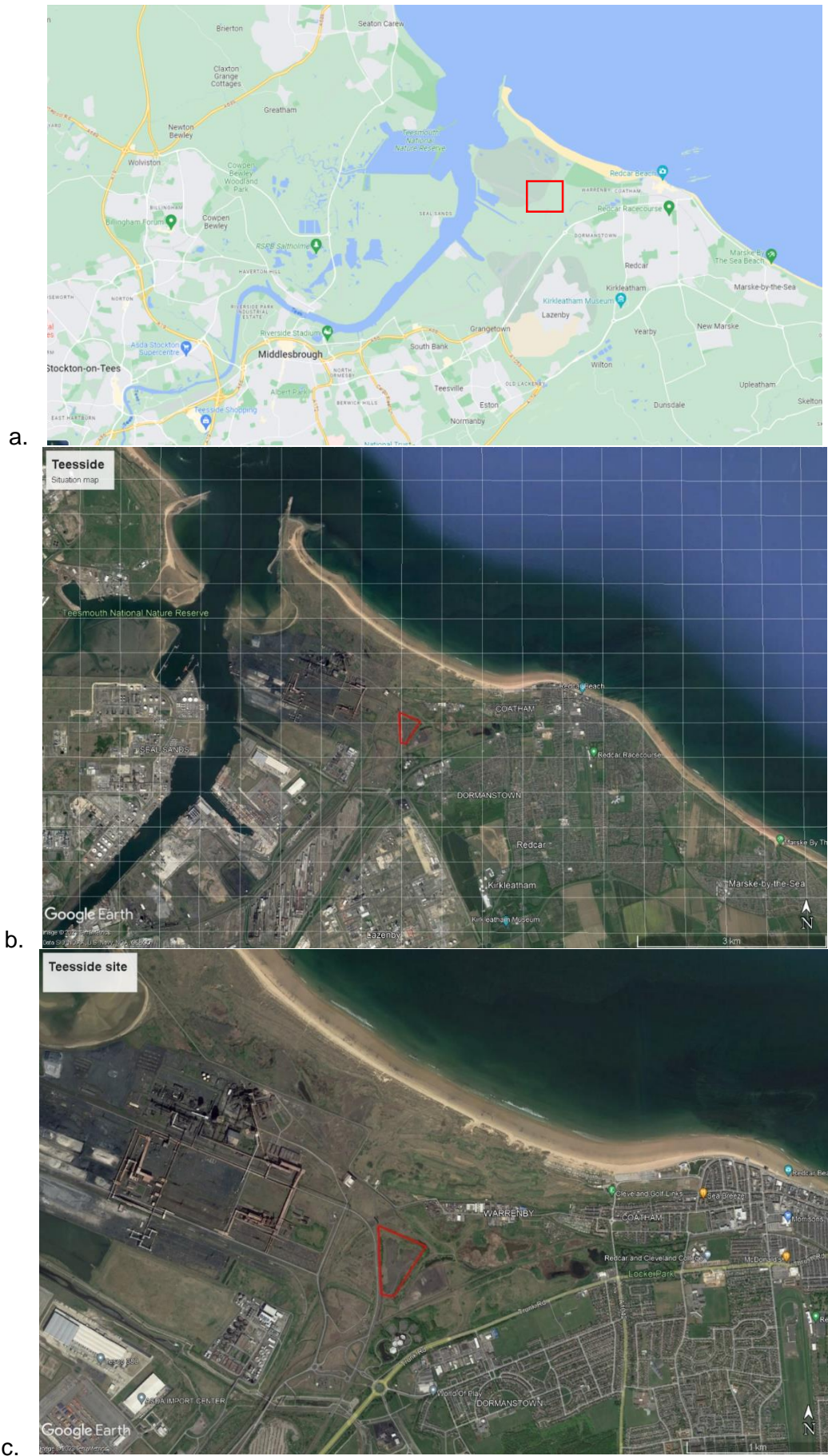


Figure 1 : General views of Teesside site, a. general traffic view (Google Maps), b. and c. Google Earth views at different scales. The red line surrounds the experimental area.

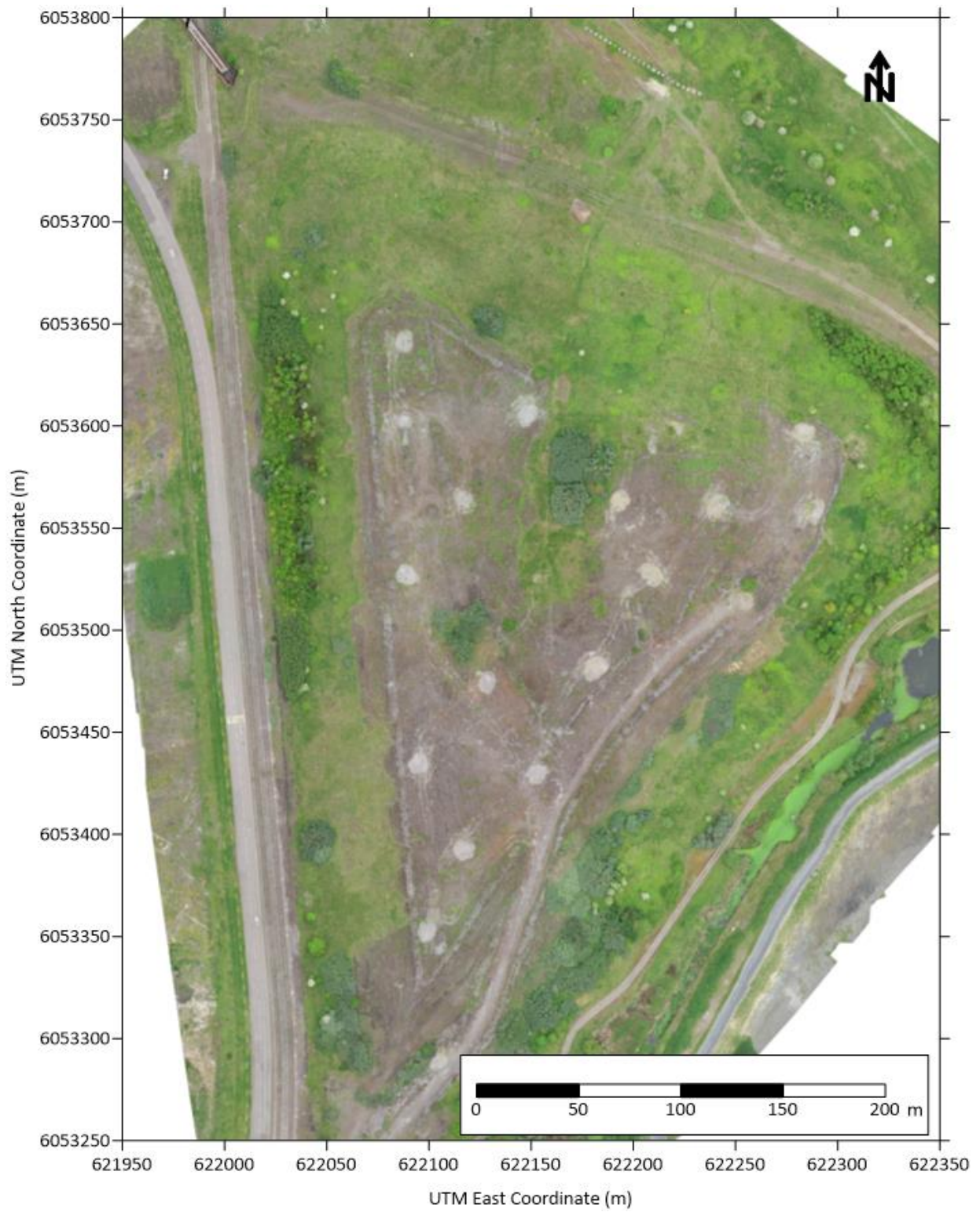


Figure 2 : Aerial view obtained with unmanned aerial vehicle (UAV) over the Teesside experimental site



a.



b.

Figure 3 : Aerial photos from Teesside area.

2.2 TOPOGRAPHY

The topography (Digital Elevation Model or DEM) of the heap has been calculated using two different techniques:

- Differential GPS measurements during geophysical survey
- Photogrammetry with UAV views

Two elevation references are presented in this project:

- AOD: Above Ordnance Datum.
- ASL: above sea level

The AOD reference is used by TEESWORKS in their reports. The ASL reference is given in export files with the software TrimbleOffice.

The comparison between the AOD and ASL references shows that the ASL reference is 5 m higher than the AOD reference.

2.2.1 DEM from GPS data

GPS positioning data from all continuous geophysical survey (Magnetic Susceptibility, DUALEM and magnetic field) have been gathered in a single file. The elevation data is restricted to the bottom of the heap. There are a few GPS measurements on heap flanks and on the natural ground surface outside the heap.

The differential correction of GPS data has been carried out using a permanent local GPS station.

The elevation data was interpolated with Surfer software (Figure 4). The mean elevation of the heap top is 20 to 21 m ASL (or 15 to 16m AOD). The mean elevation of heap bottom is 8 m ASL (or 3 m AOD).

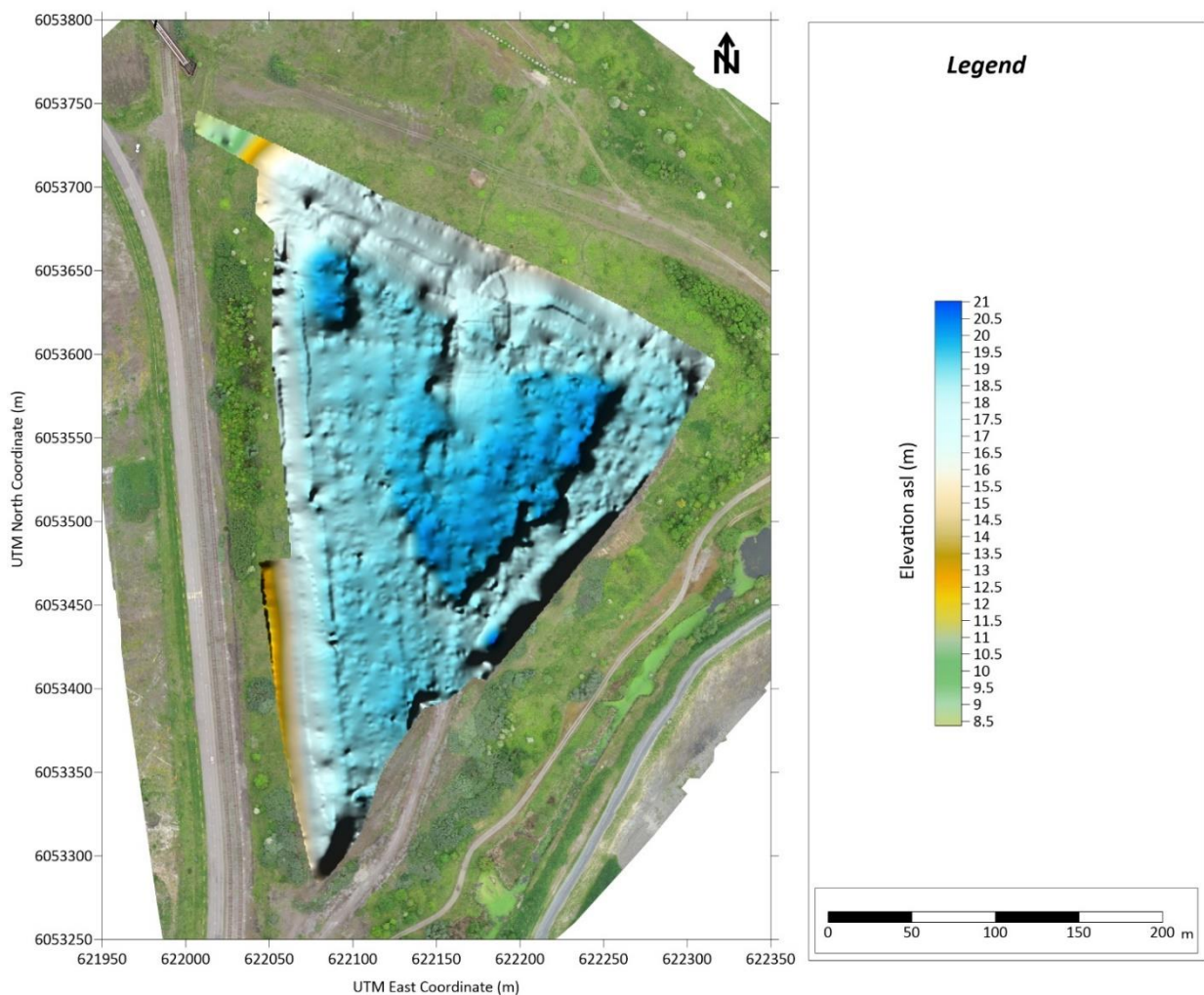


Figure 4 : Topography of Teesside site evaluated from GPS data

2.2.2 DEM from photogrammetry

Another DEM (Figure 5) was calculated from UAV photogrammetry. The topography obtained from photogrammetry has been calibrated with GPS-positioned targets on ground. Areas with high vegetation (bushes, trees) has been removed from the dataset.

The map of the difference of elevation between DEMs obtained from UAV photogrammetry and GPS data shows small differences (less than 25 cm) except around the bushes and vegetated zones (Figure 6).

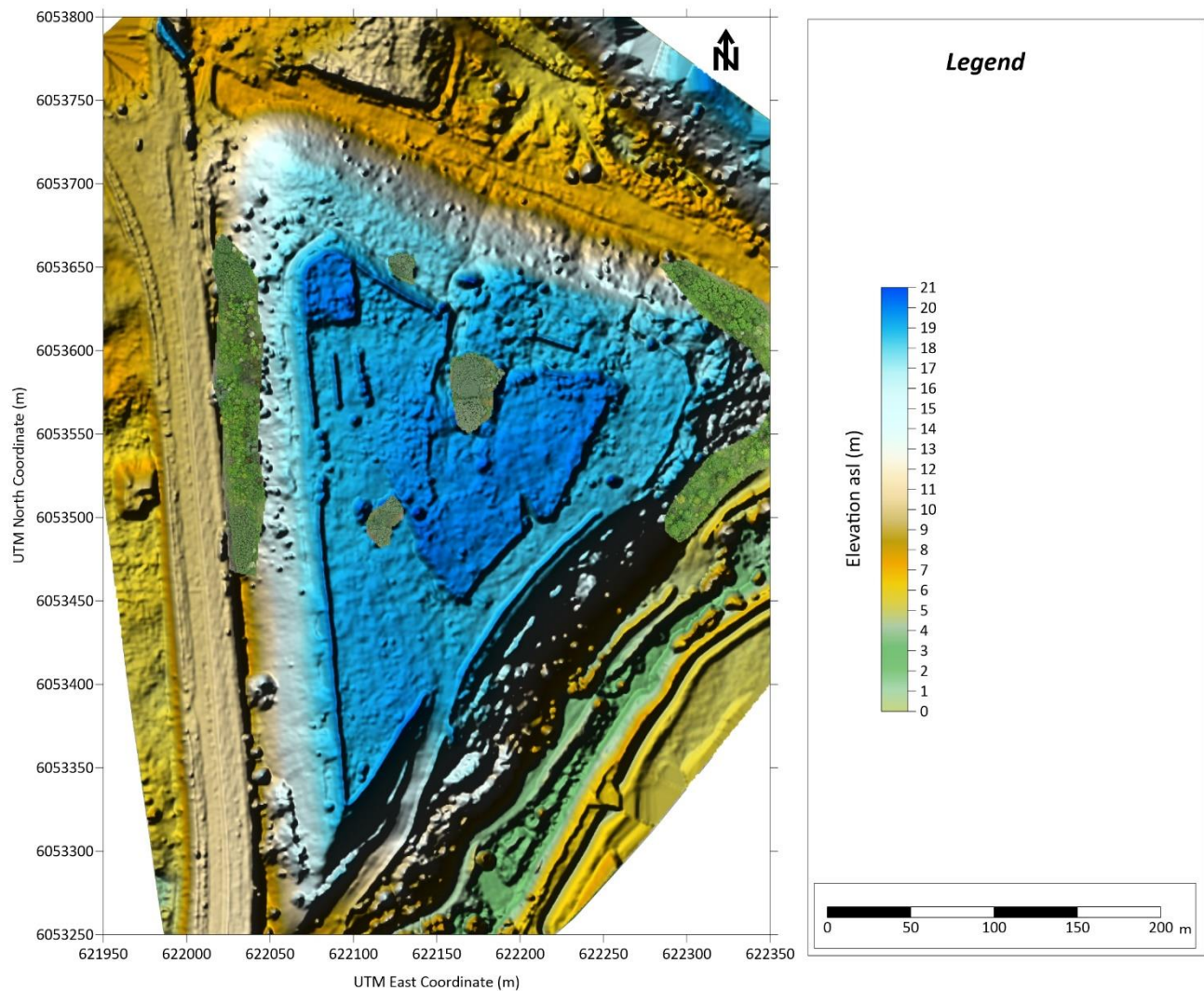


Figure 5 : DEM obtained from UAV photogrammetry

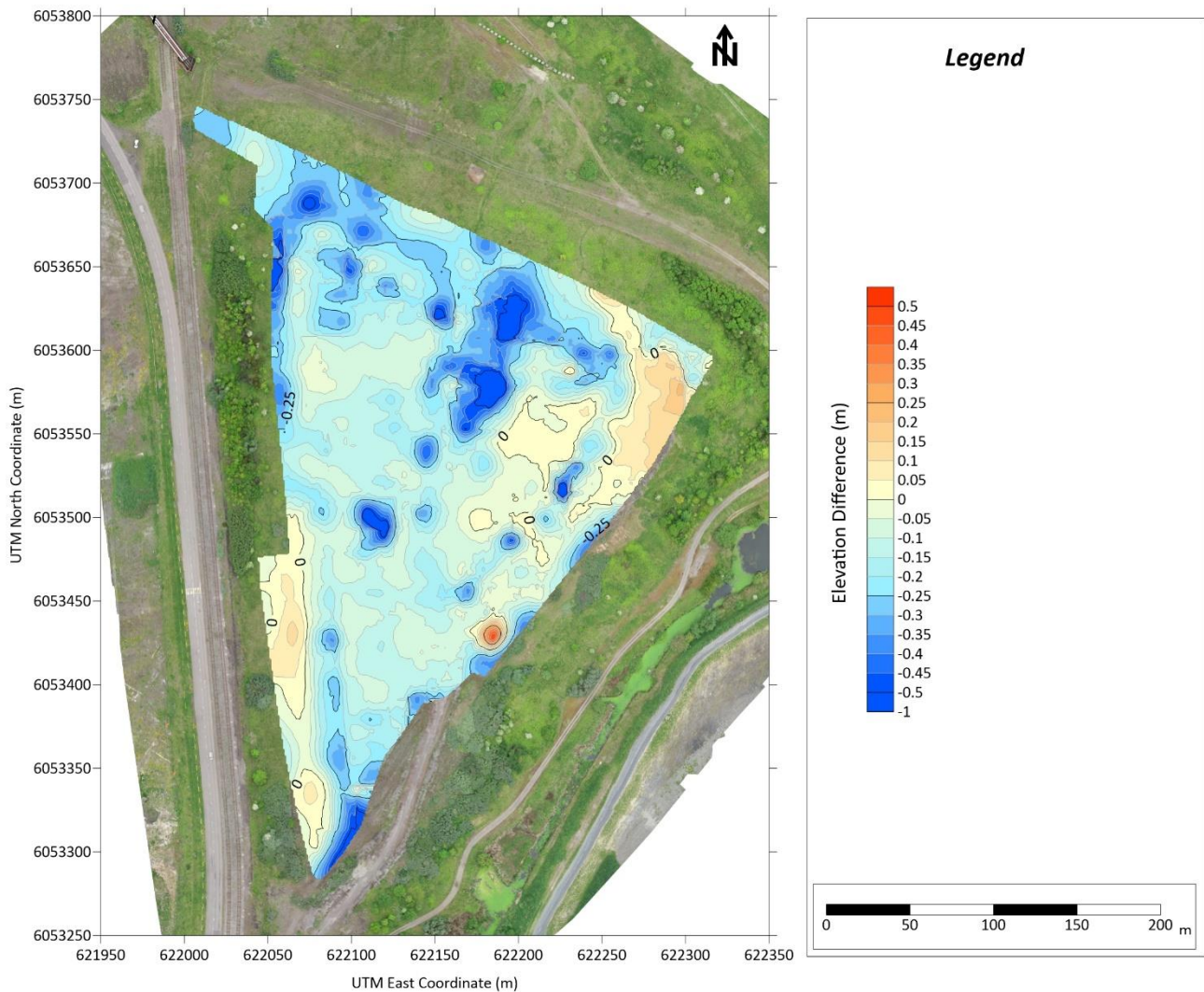


Figure 6 : Elevation difference map between UAV DEM and GPS DEM

2.3 GEOLOGICAL SETTINGS AND SITE DESCRIPTION

The mean elevation of the surrounding natural terrains is around 8m above sea level (asl), or 3m AOD. A wet zone, composed of ponds and a drainage canal, is present at the east of the heap. The water table visible in the pond is at the elevation 7m asl (or 2m AOD).

The Teesside site is situated over Quaternary Flandrian tidal flat deposits, composed of clay, silt and sands. This layer lays over Devonian glaciolacustrine deposits (Figure 7).

Figure 8 shows a typical vertical cross-section of the heap, from top to bottom:

- 10 m of landfilled wastes (from 20m asl to 10m asl – or from 15m to 5 m AOD)
- 2 to 6m of reclaimed land
- 6 to 9m of estuarine deposits (clay and sandy clays)
- The bottom medium is a lower Lias layer from -2m asl (or -7m AOD).

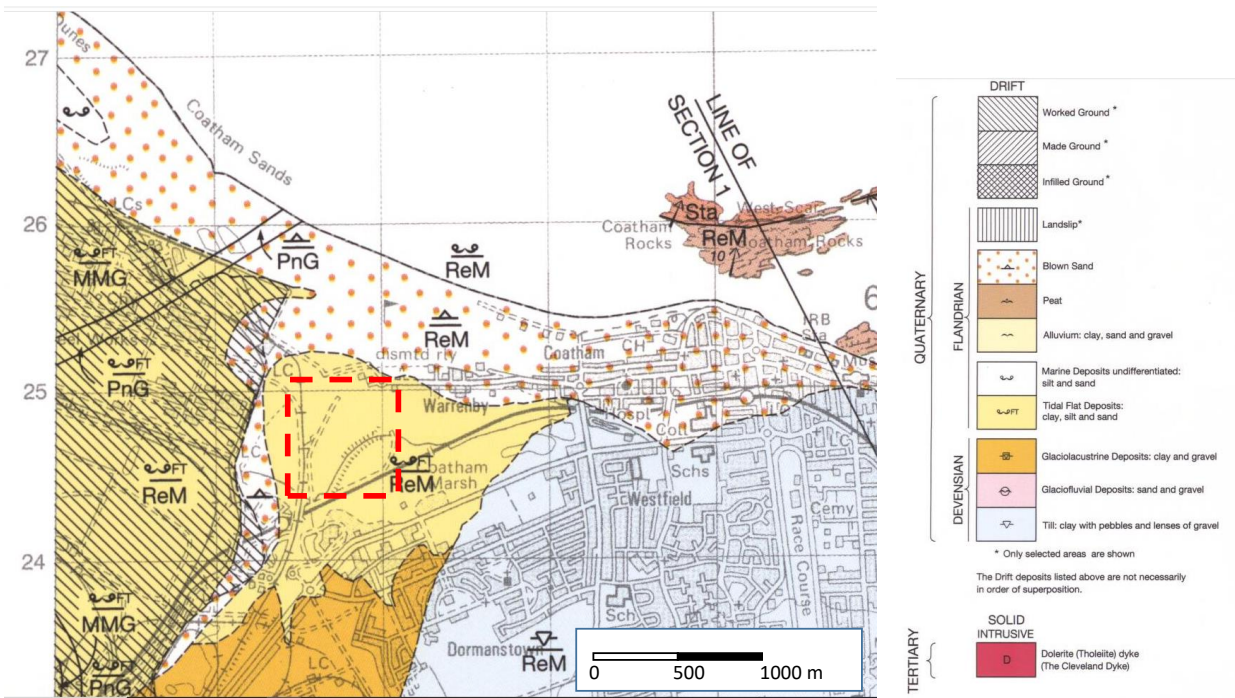


Figure 7 : Geological map of Teesside site (British Geological Survey 1/50000 map, Guisborough). The test site is surrounded by a dashed red line

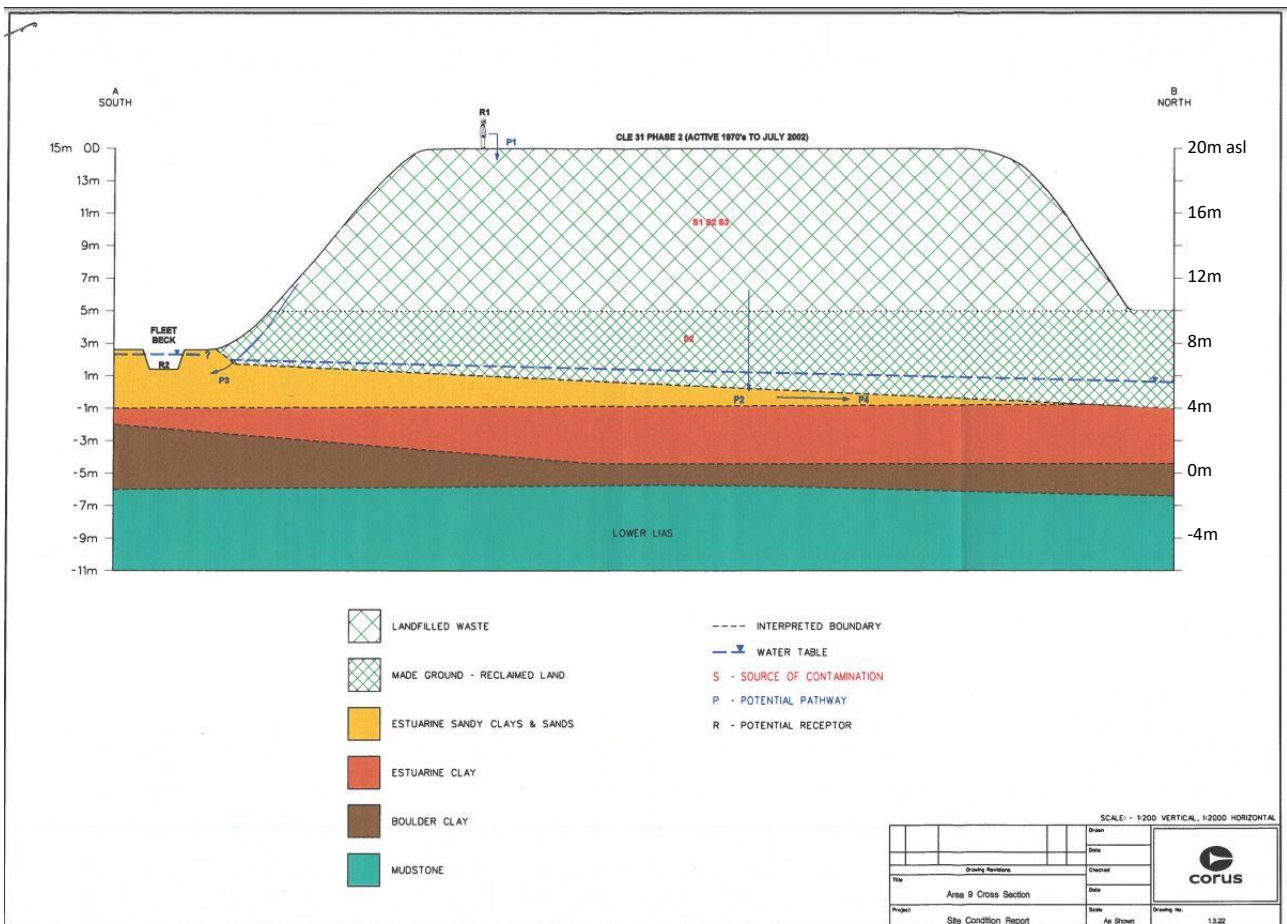


Figure 8 : Geological schematic cross-section of the survey area. The left vertical scale is the AOD (or OD) reference. The right vertical scale is the ASL reference

3 GEOPHYSICAL SURVEY

The geophysical survey was carried out from May 17th to May 25th 2022 on Teesside site.

The team for the geophysical survey was composed with (Figure 9):

- BRGM
 - o Jean-Christophe GOURRY, geophysicist engineer
 - o Alison COLOMBAIN, geophysicist technician
- University of Liège
 - o Marc DUMONT, Geophysics post-doctorate researcher
- MPI
 - o Stuart HIGSON
 - o Tutu SEBASTIAN
- University of Cransfield
 - o Niall MARSAY, PhD student



a.

b.

Figure 9 : Geophysics crew on Teesside field. A. from left to right : Tutu Sebastian, Niall Marsay, Stuart Higson, Jean-Christophe Gourry and Alison Colombain. B. from left to right : Tutu Sebastian, Niall Marsay, Stuart Higson, Marc Dumont and Alison Colombain.

3.1 GEOMAGNETIC SURVEY

3.1.1 Survey strategy and data processing

Two kinds of geomagnetic surveys have been carried out on the site :

- Measurements of the geomagnetic field amplitude (with a magnetometer)
- Measurements of surficial magnetic susceptibility (with a kappa-meter)

The geomagnetic field amplitude was measured with Geometrics G858 magnetometer, in vertical gradient mode, i.e. with two magnetic field probes one above the other, with 1 m separation. Each data was positioned with a D-GPS (decimetric precision, Trimble GEO7X with Zephyr III antenna). Magnetic field was measured continuously with 2 readings every 1s. As the operator walking speed is 1m/s, the spacing between 2 points along a profile is 0.5m. North-South profiles spacing is around 20m, and East-West profiles spacing is around 50m (Figure 10). The spacing is not constant due to access difficulties for the operator. The survey covers the whole heap top.

The surficial magnetic susceptibility points were measured with Bartington MS2D kappameter, and positioned with a decametric D-GPS (Trimble GEO7X with Zephyr III antenna, Figure 11). For each measurement, the kappameter probe is first lifted 2m from the ground (for a zero calibration) and applied at ground surface during 2 seconds for the reading. The depth of investigation of such probe

does not exceed 5 cm. The spacing between 2 points along a profile is 10m, and the spacing between profiles is around 20m (Figure 11). The survey covers the whole heap top.



Figure 10 : Magnetic field measurements points map with Geometrics G858 magnetometer

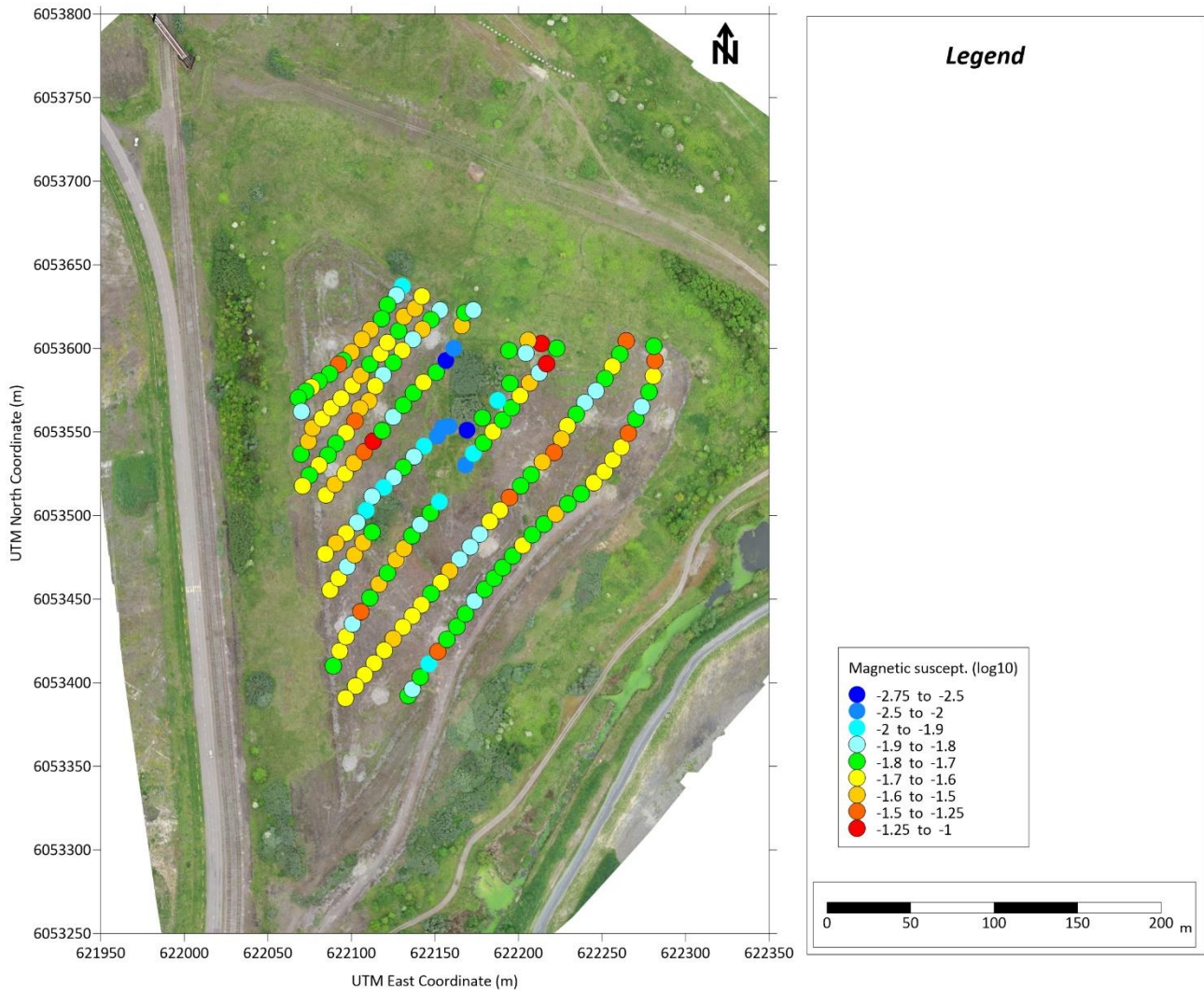


Figure 11 : Magnetic susceptibility measurement points with the Bartington MS2D kappameter

3.1.2 Results

The vertical magnetic field gradient ranges between -200 and +200 nT/m. The magnetic field gradient map (Figure 12) shows no trend, and large local variations are visible on the interpolated map. The homogeneous magnetic gradient areas have limited dimensions (less than 20x20 m). Magnetic field gradient reflects shallow variations in magnetic susceptibility up to a few meters (less than 10m). Wastes have likely variable magnetic susceptibility at decametric scale.

On the other hand, the surficial magnetic susceptibility map (Figure 13) shows three different homogeneous large areas: two high susceptibility areas (0.02 to 0.04 SI, i.e. -1.7 to -1.4 in logarithmic scale) in the east and west framing a zone of lower susceptibility (80 to 1000 SI) in the Northern-central part of the heap around the main bush. The areas of high magnetic susceptibility show local huge magnetic susceptibility reaching 0.09 SI (-1.04 in log10 scale). The wastes are composed of magnetic iron oxide such as magnetite, due to the high temperature processing. The central area is covered with topsoil that has encouraged the development of vegetation. This topsoil, which is not polluted by metallic compounds, has lower magnetic susceptibility.

The comparison of surficial magnetic susceptibility and vertical magnetic field gradient shows no correlation between these two parameters (Figure 14). While the surface waste is distributed in a locally homogeneous manner, the same waste is distributed in a much more dispersed manner on

a decametric scale. The heap is thus composed of heterogeneous wastes, with high variable magnetic properties.

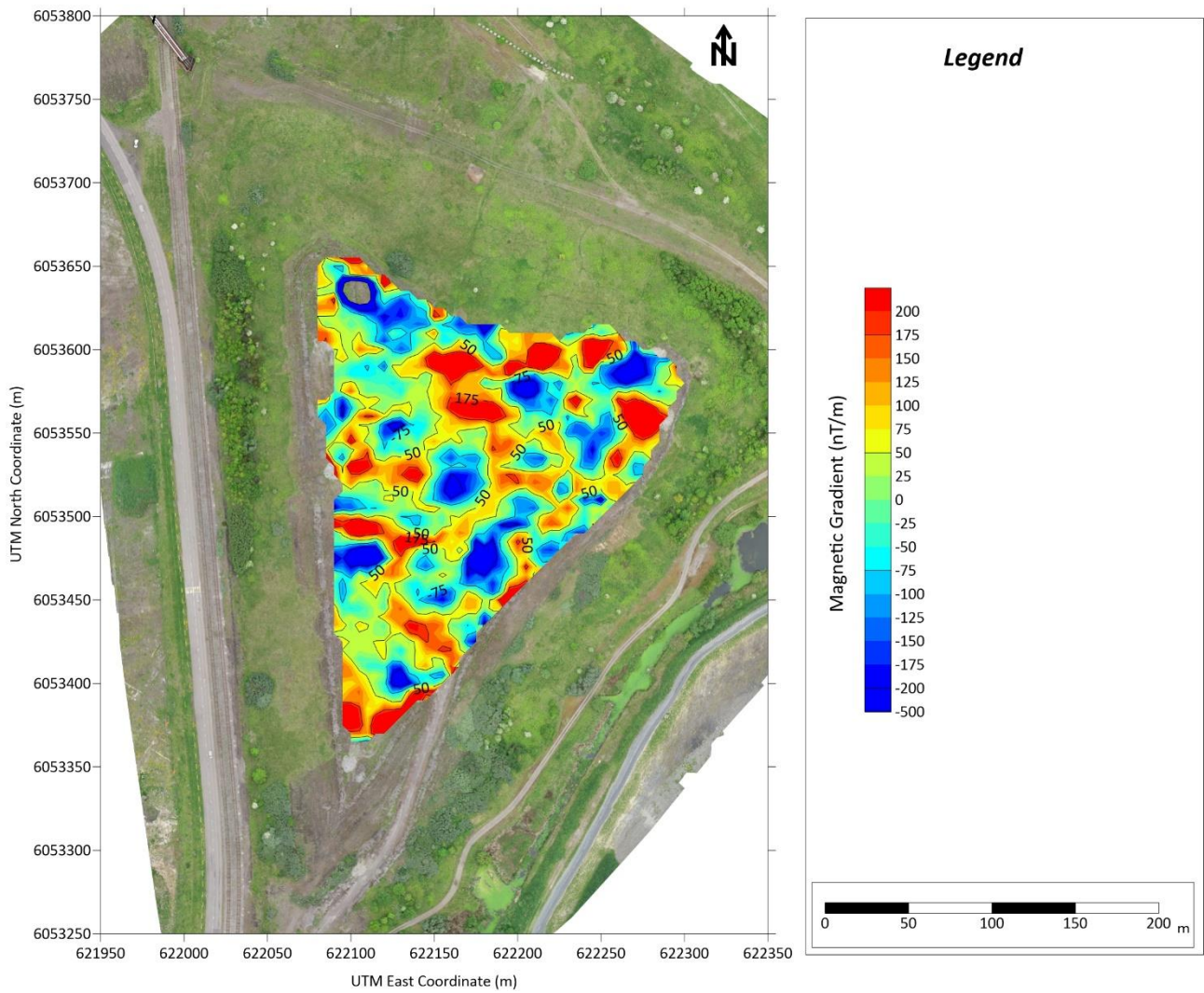


Figure 12 : Magnetic field gradient map

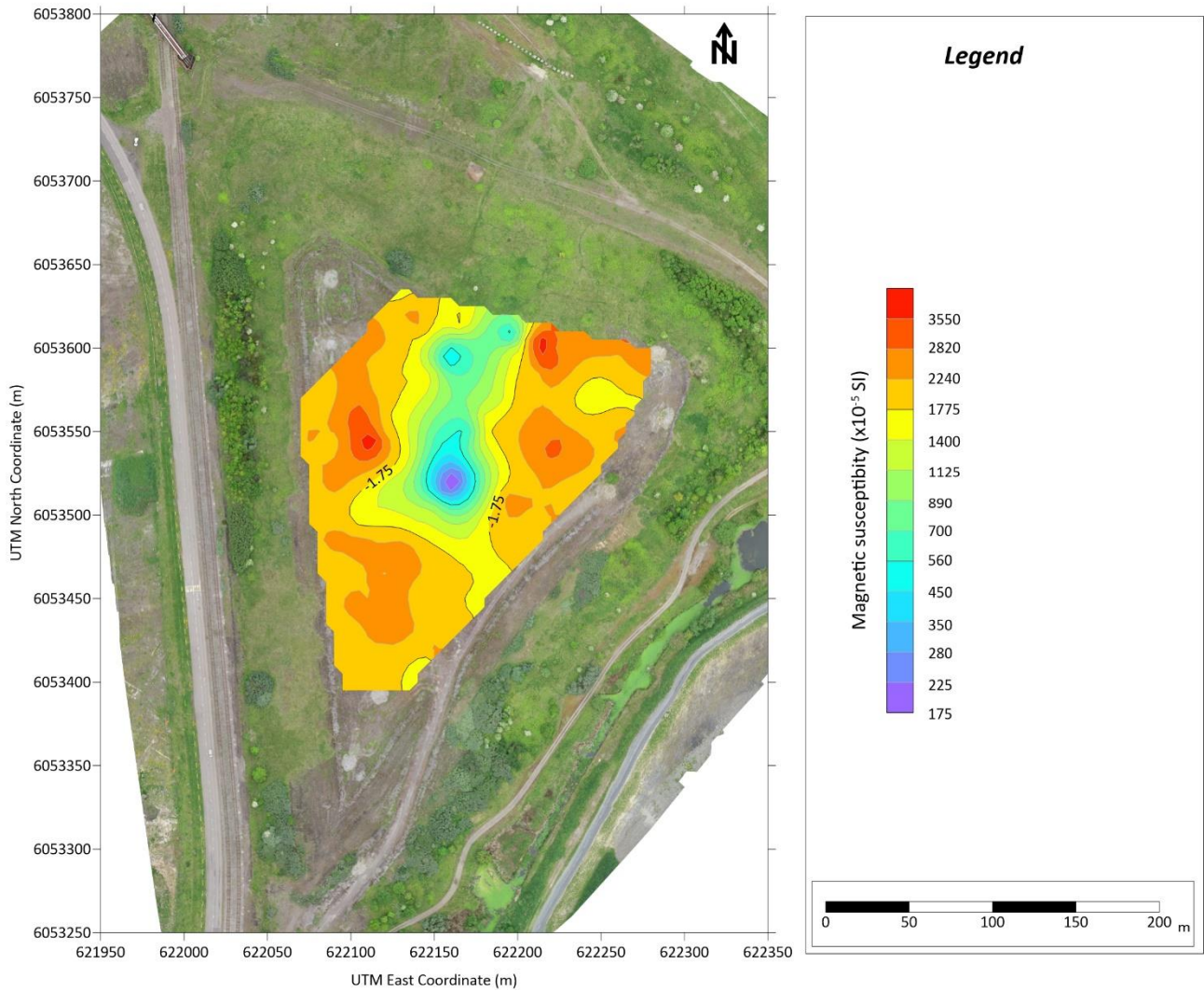


Figure 13 : Magnetic susceptibility measurement map (logarithmic scale)

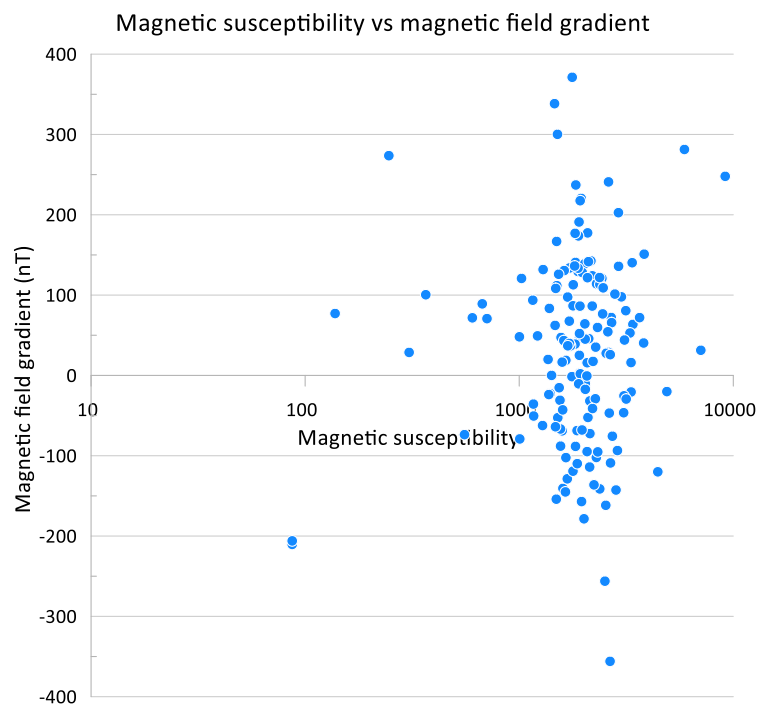


Figure 14 : Correlation graph between surficial magnetic susceptibility and magnetic field gradient.

3.2 ELECTROMAGNETIC (EMI) SURVEY

3.2.1 Survey strategy and data processing

An ElectroMagnetic Induction (EMI) survey was carried out on the top of the waste heap with a [DUALEM-421S](#) equipment (Figure 15).



Figure 15 : photography of the DUALEM421S tool on Teesside site

The DUALEM-421S equipment (Figure 16) is composed of:

- A single transmitter (Tx): a horizontal coil creating a vertical magnetic field at 9 kHz.
- 3 couples of receivers (Rx) situated a 1m, 2m and 4m apart from the transmitter;
- Each couple of receivers is composed a horizontal coil and a vertical coil whose axis is oriented in the Tx-Rx direction. The first probe measures in Horizontal-Coplanar mode (HCP) and the second probe measures on Perpendicular mode (PRP). The PRP coil is offset by 0.1m.

Each point is thus composed of 6 measurements:

- HCP 1 m (depth of investigation – DOI – around 1.5m)
- PRP 1.1 m (DOI around 0.5m)
- HCP 2 m (DOI around 3 m)
- PRP 2.1 m (DOI around 1 m)
- HCP 4 m (DOI around 6 m)
- PRP 4.1 m (DOI around 2 m).

Each measurement is composed of 2 readings:

- The out-of-phase component which is translated in electrical conductivity
- The In-Phase component which is proportional to the magnetic susceptibility

Finally, at each point, 12 readings are recorded and positioned with a D-GPS (decimetric precision, Trimble GEO7X with Zephyr III antenna).

For the survey, each profile were recorded continuously with 1 second between each measurement, i.e. 1m between each point while operators walking velocity is around 1 m/s. The spacing between

each profile is around 10m for the North-South profiles. East-West profiles were also carried out in the Northern part of the heap where access is more difficult (Figure 17). The whole heap is covered fairly evenly with the DUALEM421S equipment.



Figure 16 : Schematic details of the DUALEM421S tool

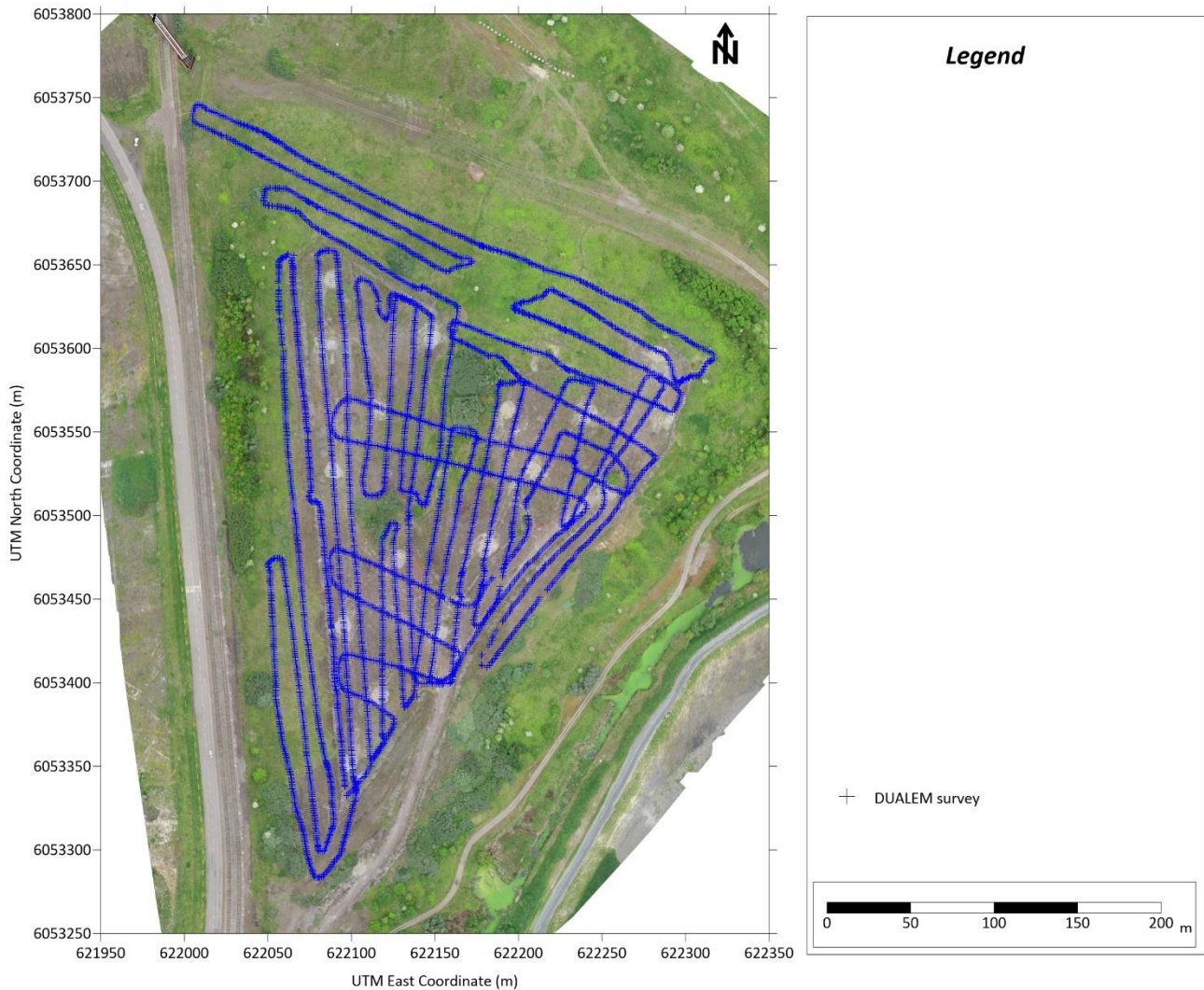


Figure 17 : DUALEM421S survey measurement points

3.2.2 Results

EMI measurements are continuous whatever the position of the instrument or its displacement. The processing requires to delete data out of the profiles and measurement bias induced by obstacle crossing. The processing is composed by 3 steps:

1. Outliers withdrawal defined by an absolute Z-score higher than 3 ($Z\text{-score} = (x - \mu) / \sigma$, where x is the observed standard value, μ the mean of the sample and σ the standard deviation of the sample). It corresponds to 0.2% of the dataset following a Normal distribution.
2. As data is oversampled along profile compared to lateral density, we decimate data by applying a reduction operation. A 1m grid is used to re-sample the data. The median of all the measurements is kept for each cell. This process smooths the data, avoiding punctual artefacts and aliasing of the interpolated maps.
3. Process a bi-harmonic spline interpolation with a minimum distance of 5 m and a damping factor of 10^{-5} . This latter is a regularization parameter ranging from 0 to 1. The higher the damping factor, the smoother the interpolation will be.

Standard EMI processing should include negative values removal. However, the high concentration of metallic content in the slag disrupt EMI measurements. This results in many negative measurements. Figure 18 and Figure 19 present the evolution of EMI dataset after each steps of the processing scheme. We clearly see mainly negative values on HCP conductivities and PRP in phase

signal. This might come from the magnetic properties of metallic component which disrupt the primary and secondary electromagnetic field. Several tests of EMI data correction have been tried but so far no relevant solution have been found.

The tests included:

- Selection of the collocated EM/ERT data.
- Transformation of the selected apparent conductivities into a quadrature EM signal
- Remodeling of the apparent conductivity using the low induction number (LIN) hypothesis and using Maxwell's equations from the FDEM1D code.

In all cases, the results were very different from the ERT data. In this condition, EMI data will be interpreted only qualitatively.

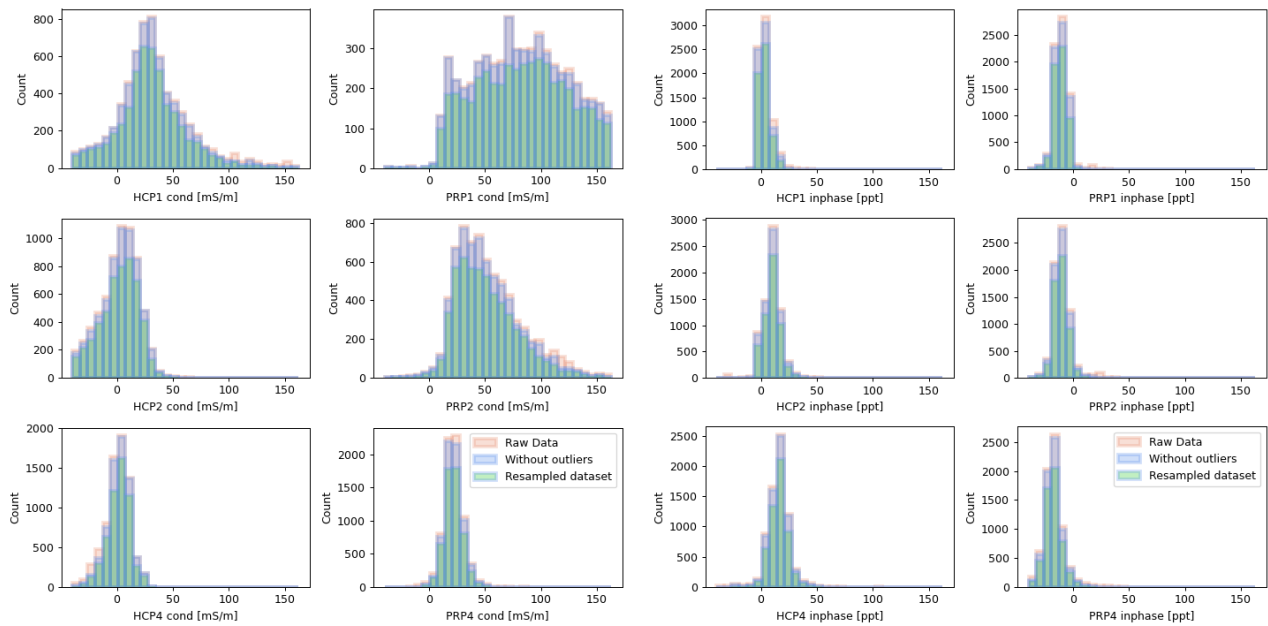


Figure 18 : Histogram of EMI data from the raw data, after outliers withdrawal and resampling.

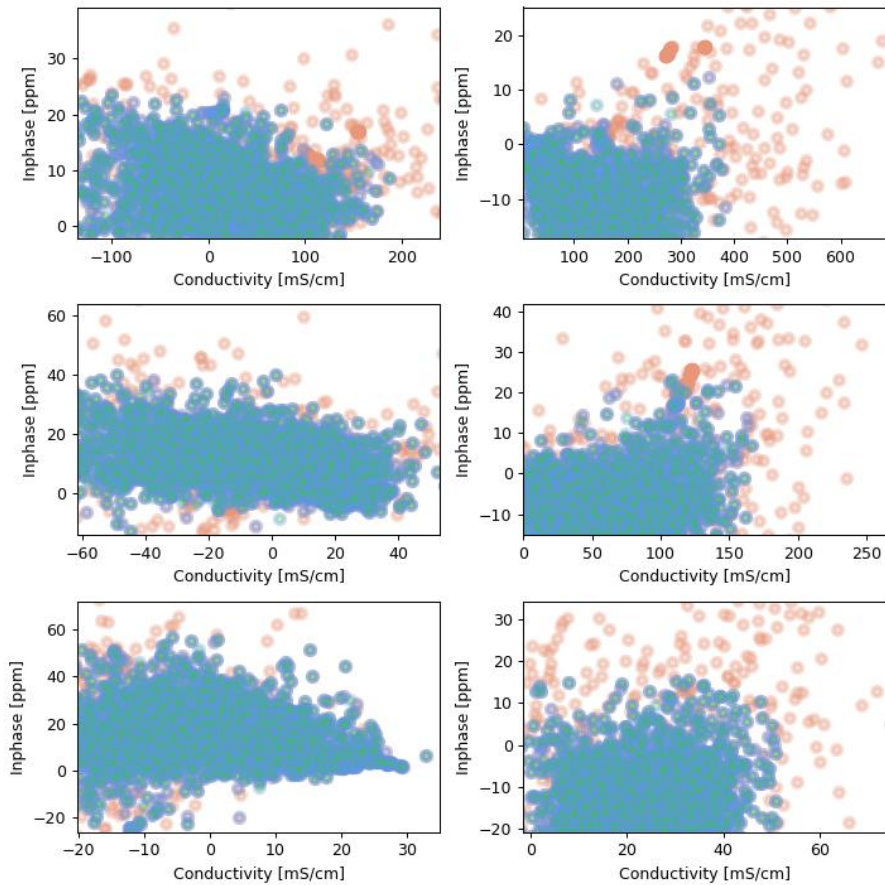


Figure 19 : Scatter plot of EMI dataset with raw data (red dots), without outliers (blue dots), and resampled dataset (green dots). This plots allow to see the value of removed dataset.

As a result, we obtain 12 maps for the signals (conductivity and in phase signal). Figure 20 and Figure 21 presents the 6 electrical conductivity from EMI mapping. The maps are divided in function of the coil set-up, HCP or PRP, as the sensitivity are different. For each maps, the estimated depth of investigation is specified.

At shallower depth (0.5 and 1 m) a large negative area is present in the slopes of the slag and the area with vegetation at the north. The rest of the slag appear mainly conductive.

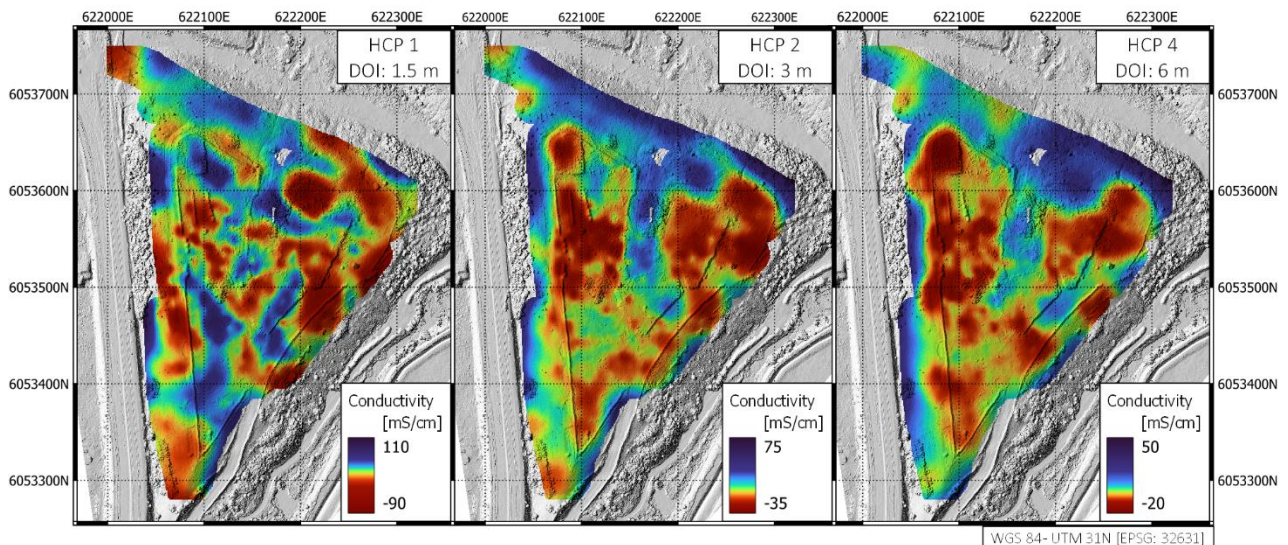


Figure 20 : Ground electrical conductivity from HCP coils.

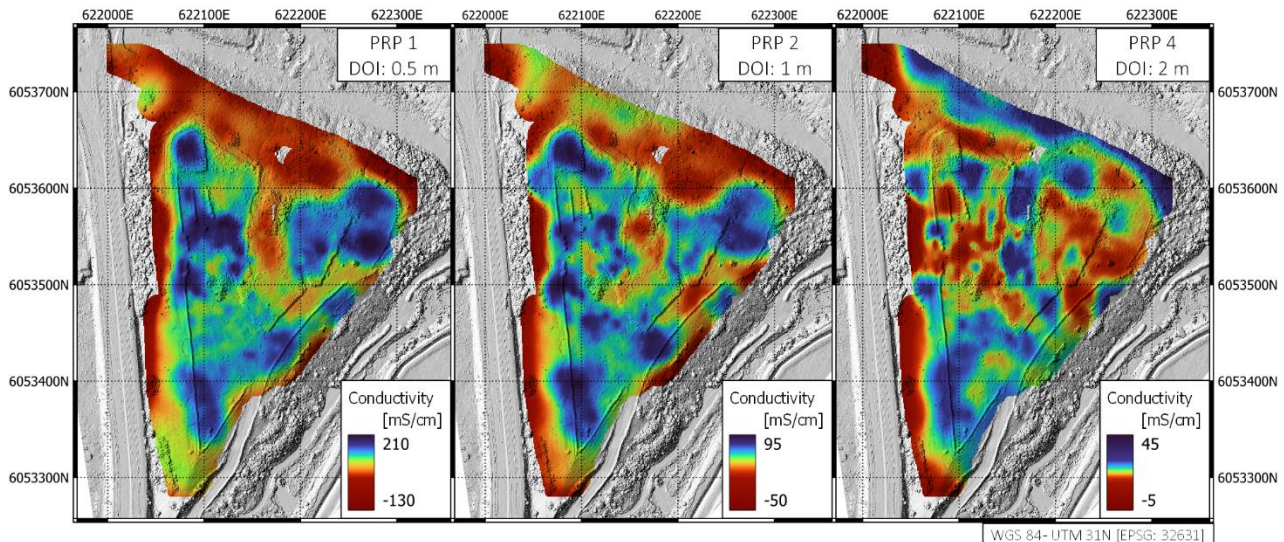


Figure 21 : Ground electrical conductivity from PRP coils.

The calculation of the apparent conductivity for each component is based on the Low Induction Number (LIN) approximation (Mc Neil, 1980). In the present case study, the LIN approximation is not valid because of the high magnetic susceptibility and high chargeability.

In the present case study, the LIN approximation is not respected and the apparent conductivity is no more proportional to the true field conductivity. In other words, out of the LIN approximation, the magnitude and sign of the secondary magnetic field is not linear with the field conductivity. In this context, apparent conductivity can be negative in HCP configuration. Moreover, for the same depth of investigation, apparent conductivity in PRP configuration can be much higher than apparent conductivity in HCP configuration.

The EM signals between 1.5 and 2 m depths (DOI) are heterogeneous. This is a consequence of wastes with high magnetic susceptibility as shown by the magnetic survey (see chapter 3.1.2), as surficial magnetic susceptibility influences EMI measurements.

Therefore no geometry of homogeneous material could be defined based on EMI survey. At higher depths (3 – 6 m), the slope and the area with vegetation are conductive while the rest of the slag is more resistive (or with negative values). These maps clearly highlight a difference between the slopes and the area with vegetation compared to the rest of the slag. Within the slag, EMI maps did not bring out any major pattern. Slags look heterogeneous. In order to bring a better understanding of the slag structure, ERT and IP measurements are needed.

3.3 ELECTRICAL RESISTIVITY AND INDUCED POLARIZATION TOMOGRAPHY SURVEY

3.3.1 Survey strategy and data processing

Five Electrical Resistivity and Induced Polarization (IP) tomography profiles (Figure 22) were carried out on Teesside site:

- ERT1, 225m long, orientation West-East
- ERT2, 475 m long, orientation North-South
- ERT3, 350 m long, orientation North-West / South-East
- ERT4, 350 m long, orientation North-South
- ERT5, 225 m long, orientation North-South.

The profiles were positioned so that the entire pile was covered evenly and each profile cut through the heap. Each tomography was composed of 96 electrodes, with an electrode spacing of 2.5 m, i.e. 237.5 m long. ERT2, ERT4 and ERT5 are about parallel and oriented N-S. ERT1 is oriented W-E. Profile ERT3 is oriented NW-SE and crosses the other profiles. ERT1, ERT2 and ERT4 cross each other at the same point.

This configuration allows to image deep enough to reach the natural ground below slags. Unfortunately, the southern part of the slag was too tight to set-up a West-East profile. In the longer parts, ERT/IP profiles were acquired using “roll-alongs” of the half-length (i.e. the 48 first electrodes of the profiles are installed at the end of the profile for continuing the tomography).

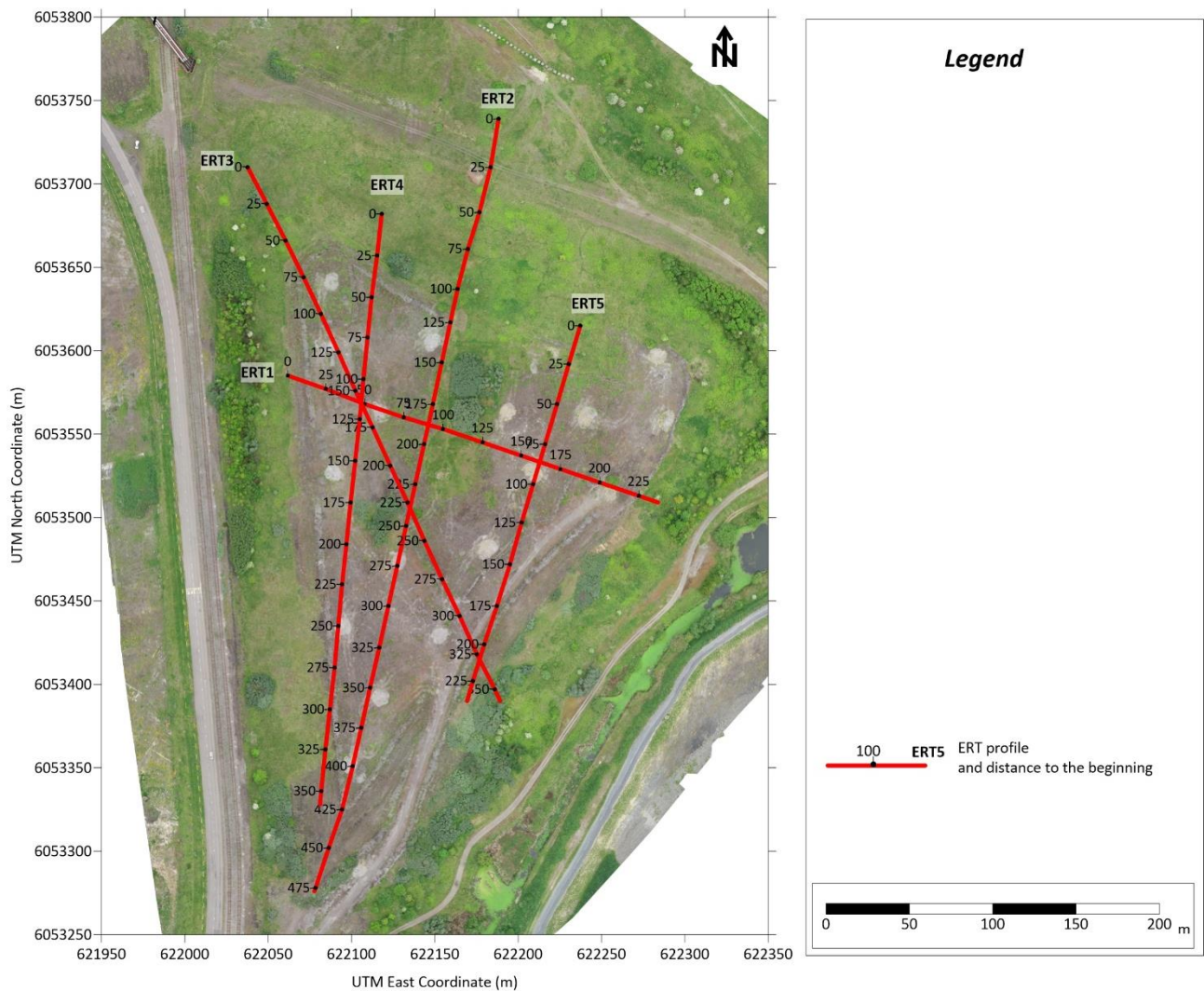


Figure 22 : Position of the 5 ERT profiles on Teesside site

The Dipole-Dipole configuration was applied for all profiles, in resistivity and IP modes (2000 ms signal period) with a Syscal Terra from Iris Instruments (Figure 23). A Wenner-Schlumberger configuration was also carried out in rho mode only (250 ms signal period). The contact resistance of each electrode was very diverse (from a few Ohm to tens of kΩ) due to changing surficial conditions (see Figure 24). It was necessary to add brine water at each electrode to lower and balance the contact resistance along each profile.



Figure 23 : Photo of the Syscal Terra equipment used for the Electrical Resistivity and IP Tomography survey



Figure 24 : Photographies of the ERT equipment on the Teesside site, in a vegetated area (left) and on a coarse-grained material (right)

3.3.2 ERT/IP processing

Data collected were first filtered by removing all measurements characterized by a repetition error on the measured resistance greater than 5%. Then, to weight the data in the inversion process, an error model was imposed with an absolute error of $10^{-3} \Omega \cdot m$ and a relative error of 3% (see Slater et al. 2000). For IP measurements, an error model has been estimated using Flores Orozco et al. (2018) model.

The weighted data were inverted with pyBERT and pyGIMLi python libraries (Günther, Rücker, and Spitzer 2006; Rücker, Günther, and Wagner 2017) using a robust constraint on the data and a blocky constraint on the model (L1 norm). The cost function of pyBERT inversion is the error weighted χ^2 . The objective value is $\chi^2 = 1$ meaning that the data are fitted to their error level. If the score is above one, the error model underestimates the real error in the data, so the inversion overfits the data. In the contrary, when $\chi^2 < 1$, the error model overestimates the real error in the data so the inversion underfits the data. The five ERT/IP profiles are presented in Figure 25 to Figure 29. For each profile, the ERT inversion present the resistivity model inverted and the IP inversion correspond to the chargeability model.

The data from the 5 profiles was also inverted with Res2DInv software (Seequent), using a robust (L1-norm) inversion technique. Results obtained with this software are slightly different from those obtained with pyBERT software (see Figure 32 to Figure 36).

On each figure, the electrical resistivity is represented on top, the electrical chargeability is represented in the middle of the figure.

A third parameter has been calculated on the basis of resistivity ρ and chargeability M parameters: the Metal Factor MF. The Metal Factor is calculated as follows:

$$- \quad MF = M / \rho$$

Where ρ is the resistivity in Ohm.m, and M is the Chargeability in mV/V (or ‰). MF is then expressed in mS/m.

The Metal Factor is used to characterize metallic ores, which are conductive and highly chargeable. Usually, the chargeability is low when the medium is conductive. The Metal Factor is representative of chargeable and conductive material, such as wastes containing metallic compounds high rate.

The Metal factor parameter is represented at the bottom of each figure.

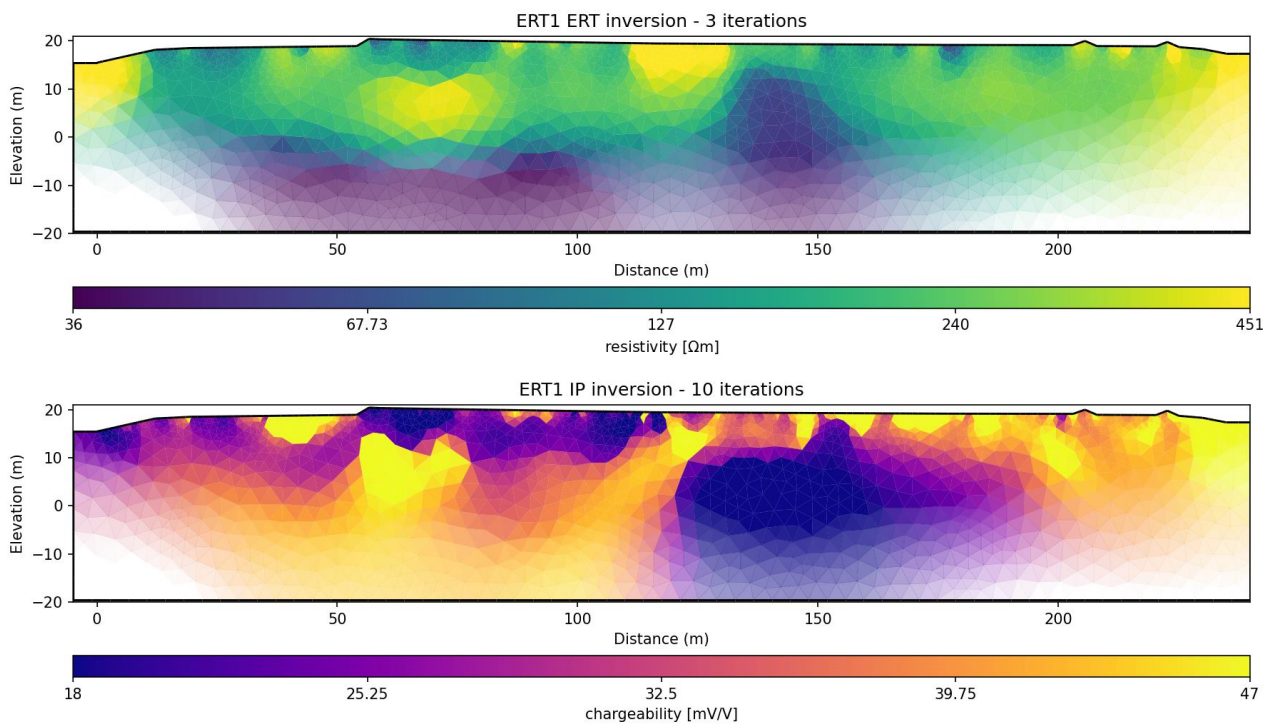


Figure 25 : Electrical resistivity (top) and chargeability (bottom) models obtained in ERT1. Both profiles are blanked below the sensitivity limit (threshold = -2). pyBERT inversion results

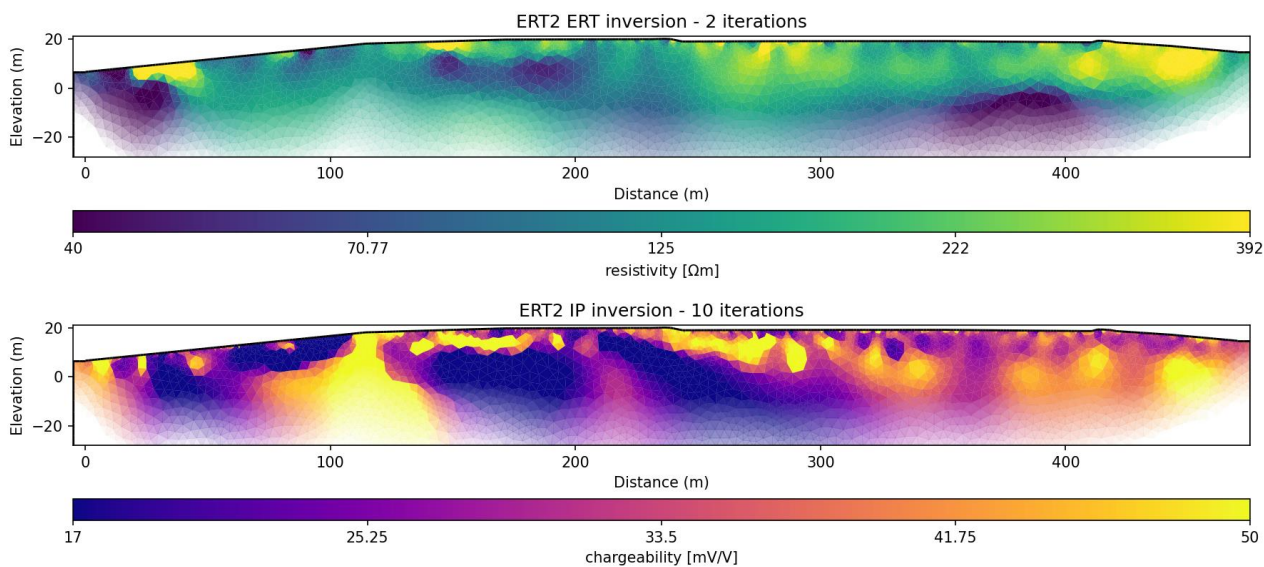


Figure 26 : Electrical resistivity (top) and chargeability (bottom) models obtained in ERT2. Both profiles are blanked below the sensitivity limit. In this profile (threshold = -2), data around 100 m of distance have been biased during the acquisition. The resistivity and chargeability obtain between 80 and 120 m of distance came from the interpolation of surrounding values. The high chargeability anomaly should be considered as an artefact. . pyBERT inversion results

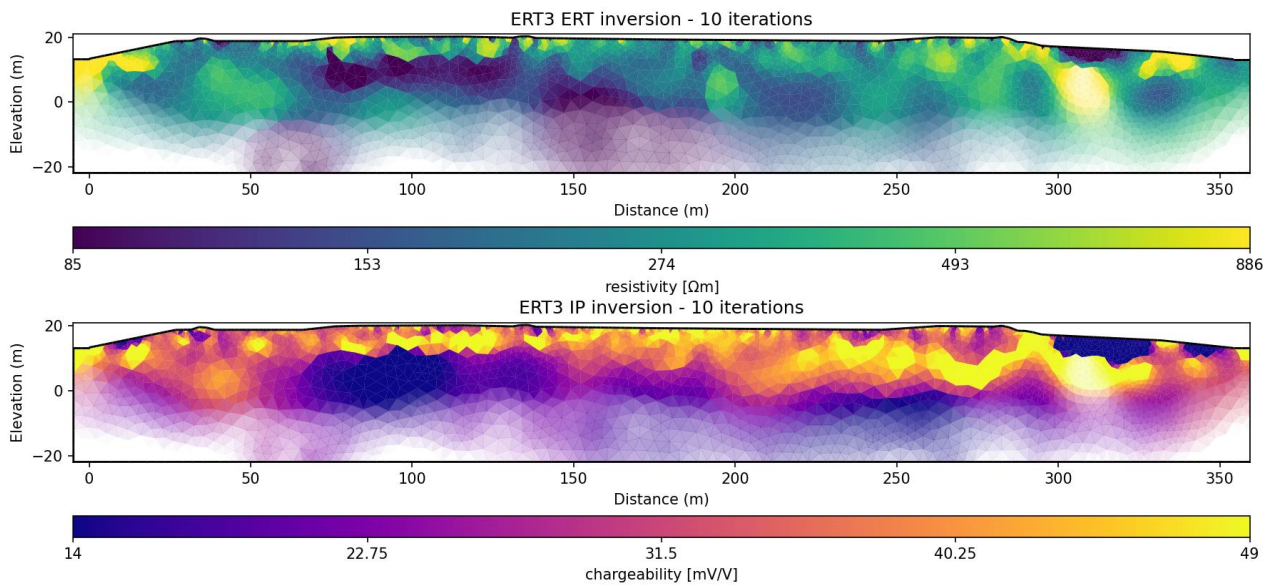


Figure 27 : Electrical resistivity (top) and chargeability (bottom) models obtained in ERT3. Both profiles are blanked below the sensitivity limit (threshold = -2). pyBERT inversion results

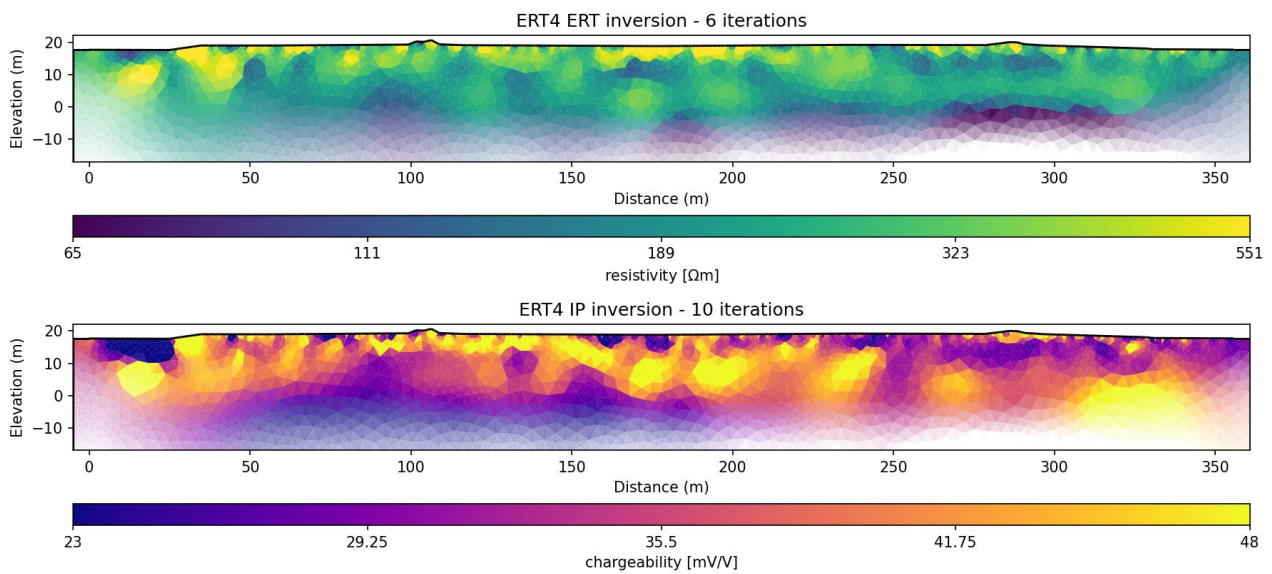


Figure 28 : Electrical resistivity (top) and chargeability (bottom) models obtained in ERT4. Both profiles are blanked below the sensitivity limit (threshold = -2). pyBERT inversion results

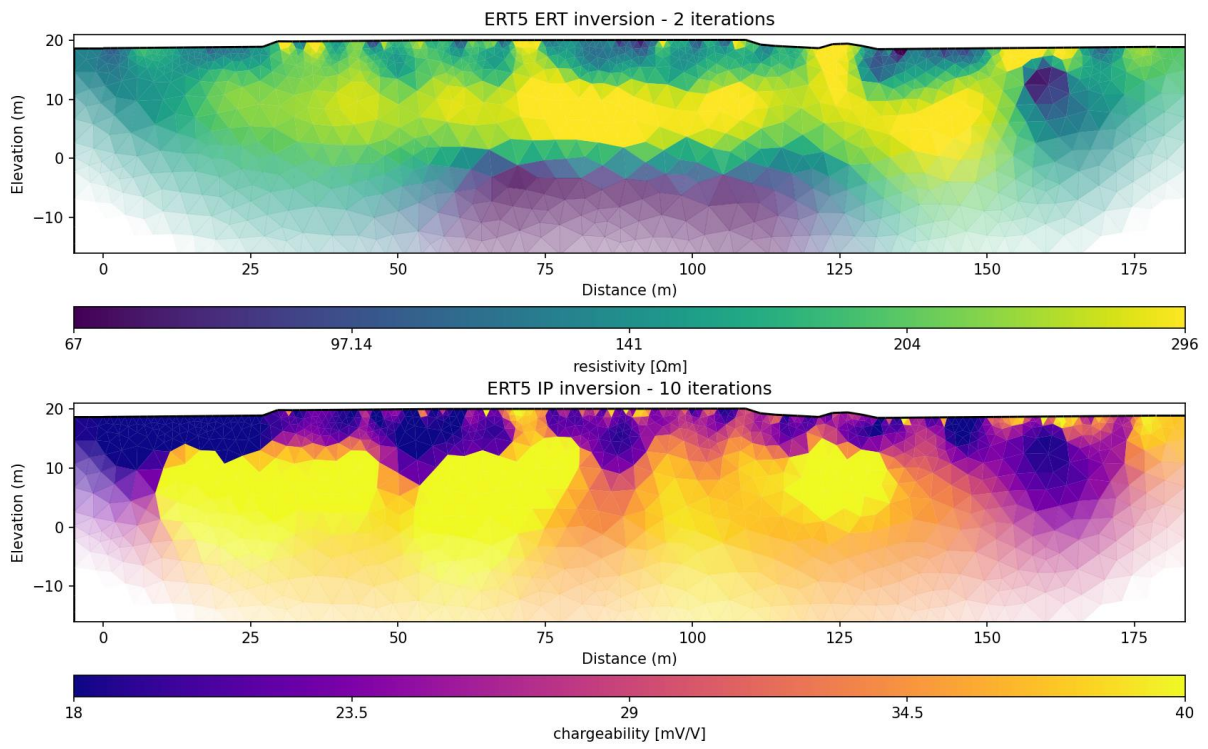


Figure 29 : Electrical resistivity (top) and chargeability (bottom) models obtained in ERT5. Both profiles are blanked below the sensitivity limit (threshold = -2). pyBERT inversion results

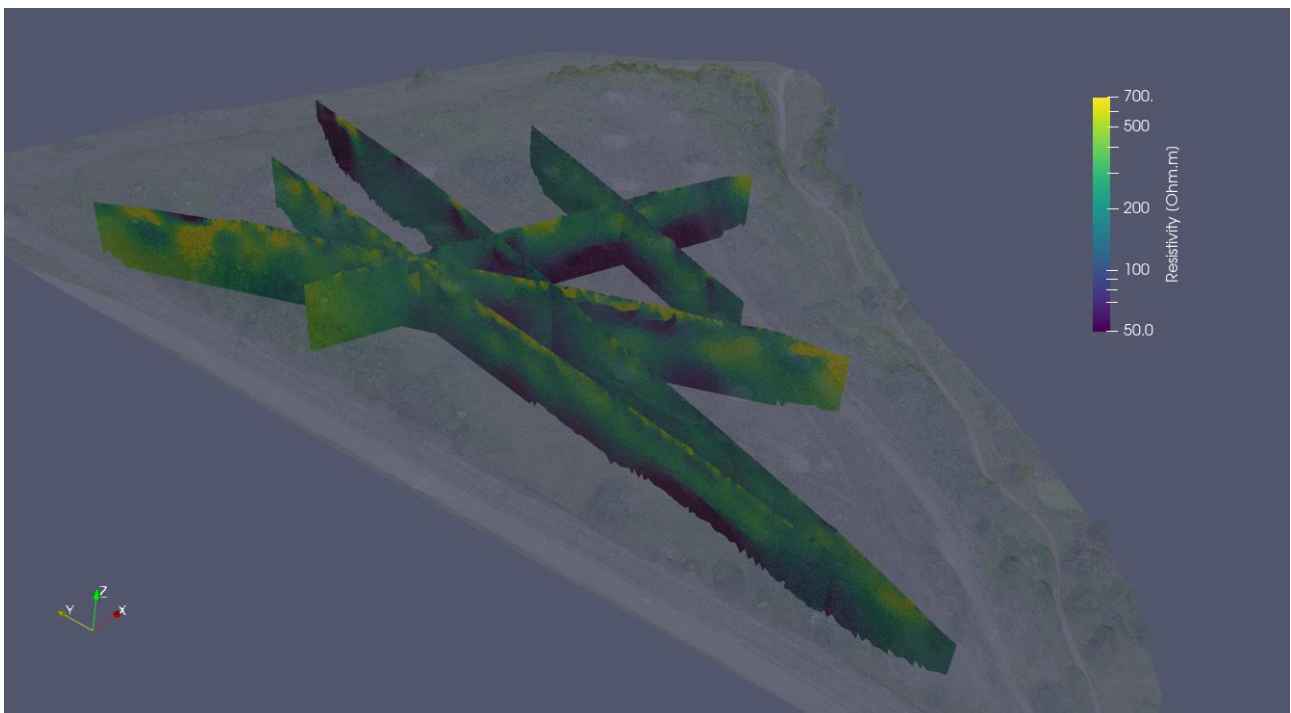


Figure 30 : 3D view of the 5 resistivity profiles covered by the digital surface model.

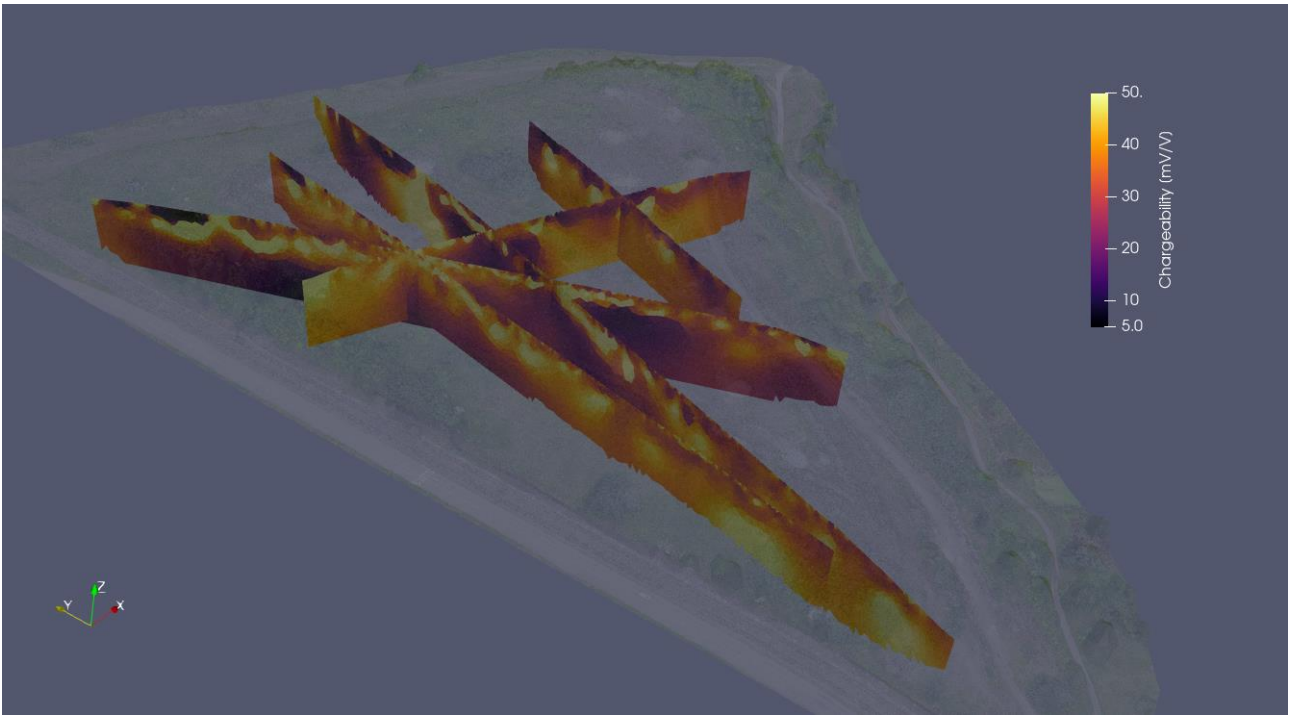


Figure 31 : 3D view of the 5 chargeability profiles covered by the digital surface model.

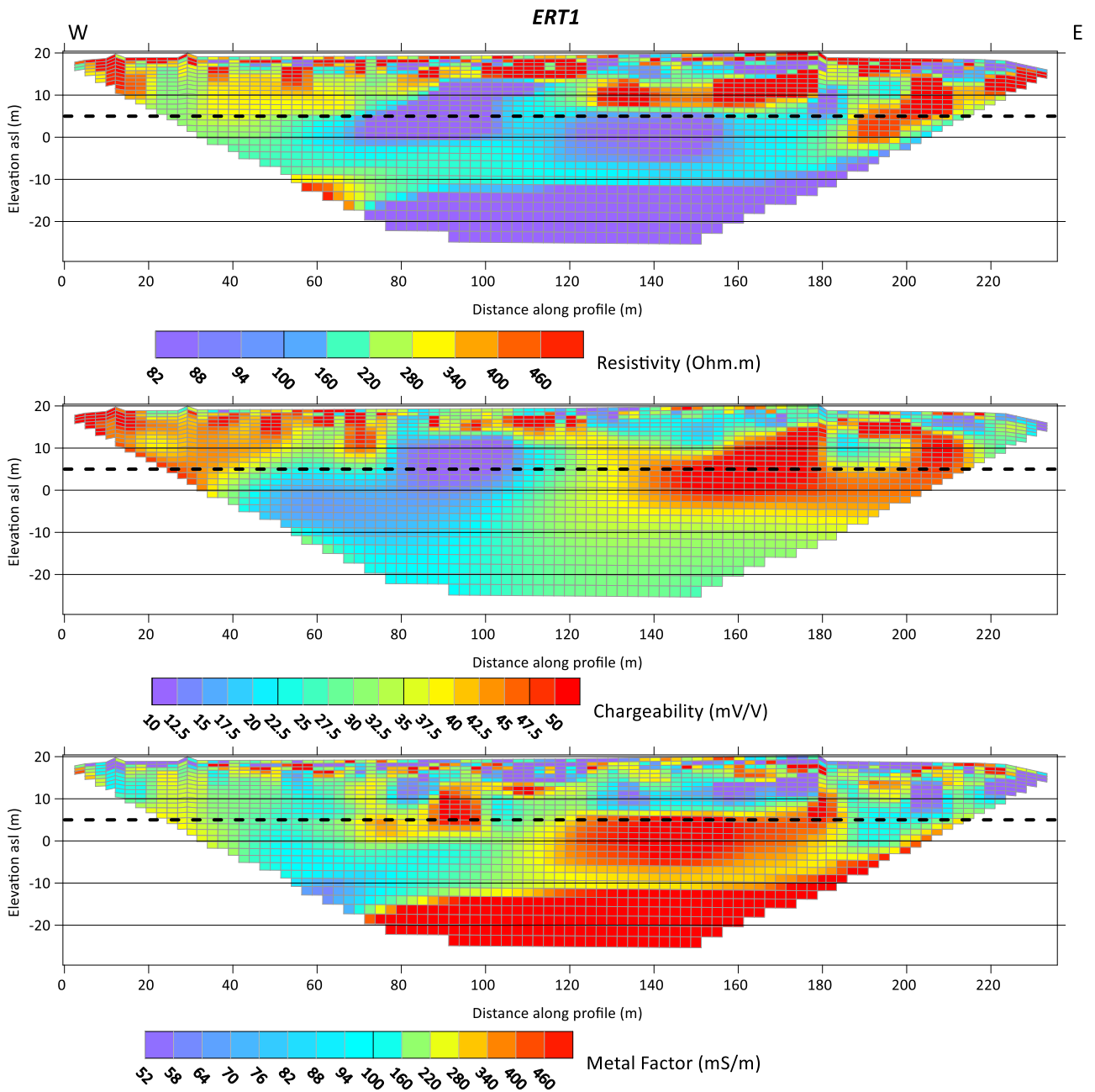


Figure 32 : ERT1.tomography. Top : Electrical resistivity cross-section, middle : Chargeability cross-section, bottom: Metal Factor cross-section. Dash black line represents the mean elevation of the heap bottom. Res2Inv inversion results.

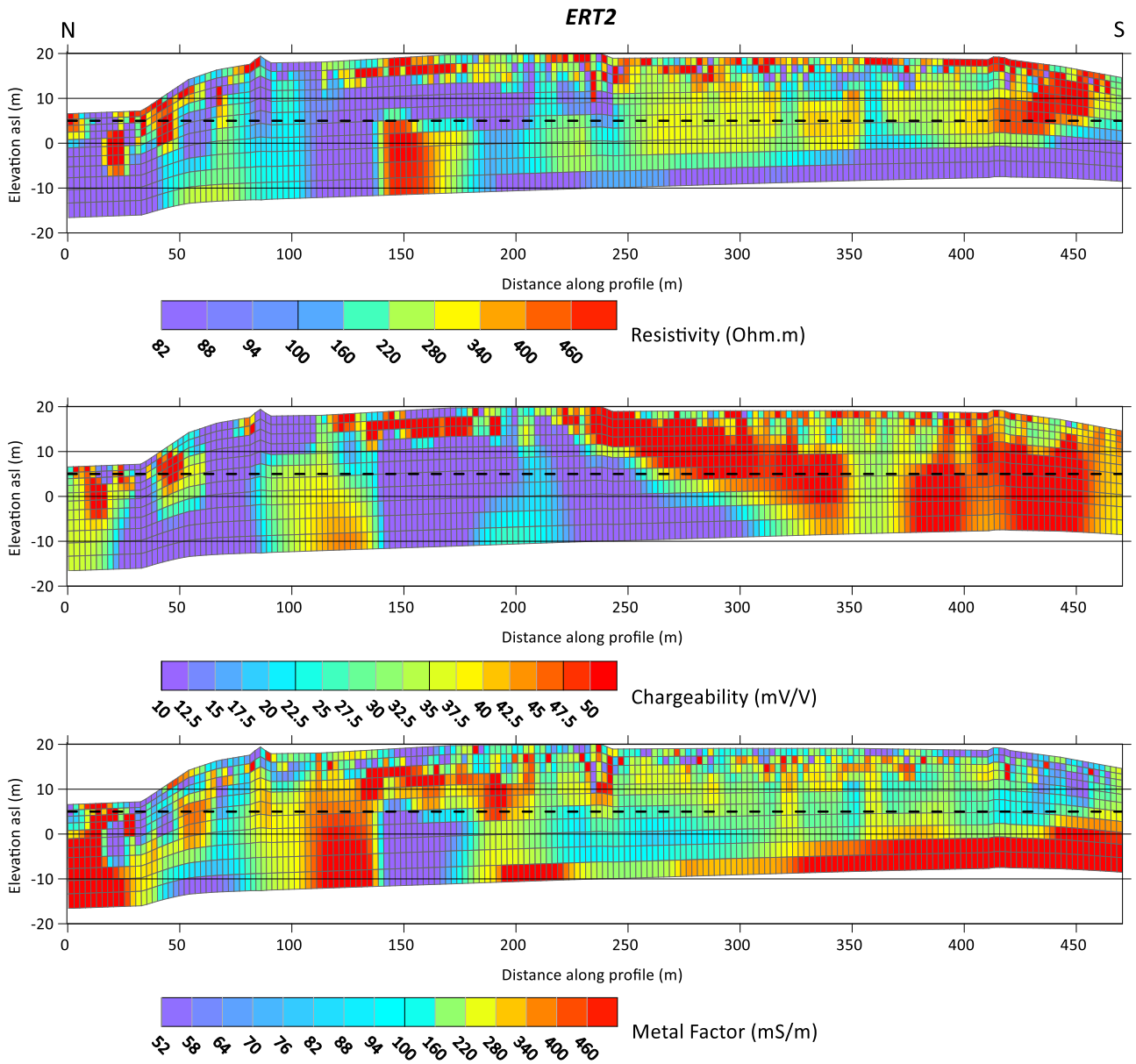


Figure 33 : ERT2.tomography. Top : Electrical resistivity cross-section, middle : Chargeability cross-section, bottom: Metal Factor cross-section. Dash black line represents the mean elevation of the heap bottom. Res2Inv inversion results.

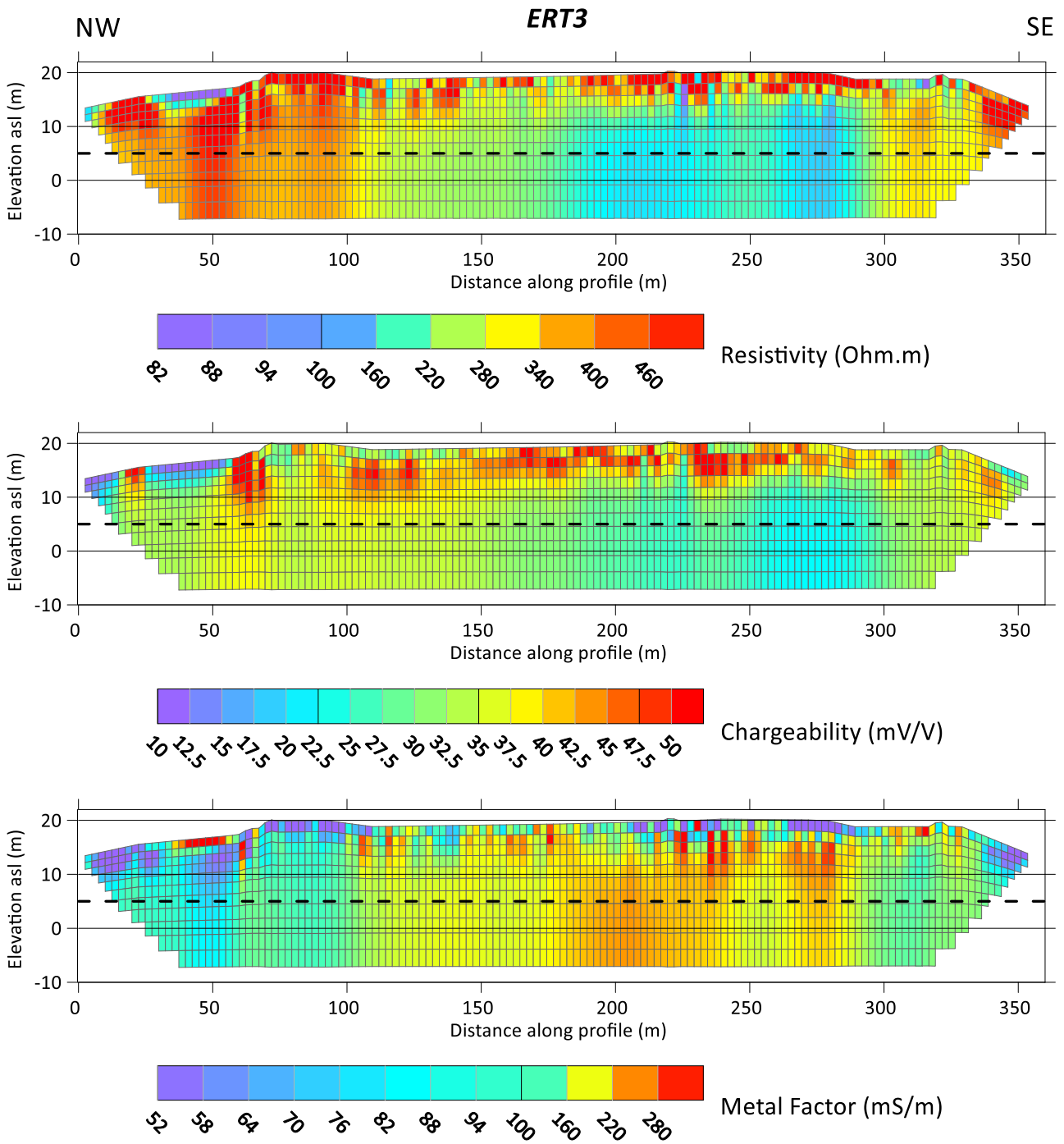


Figure 34 : ERT3 .tomography. Top : Electrical resistivity cross-section, middle : Chargeability cross-section, bottom: Metal Factor cross-section. Dash black line represents the mean elevation of the heap bottom. Res2Inv inversion results.

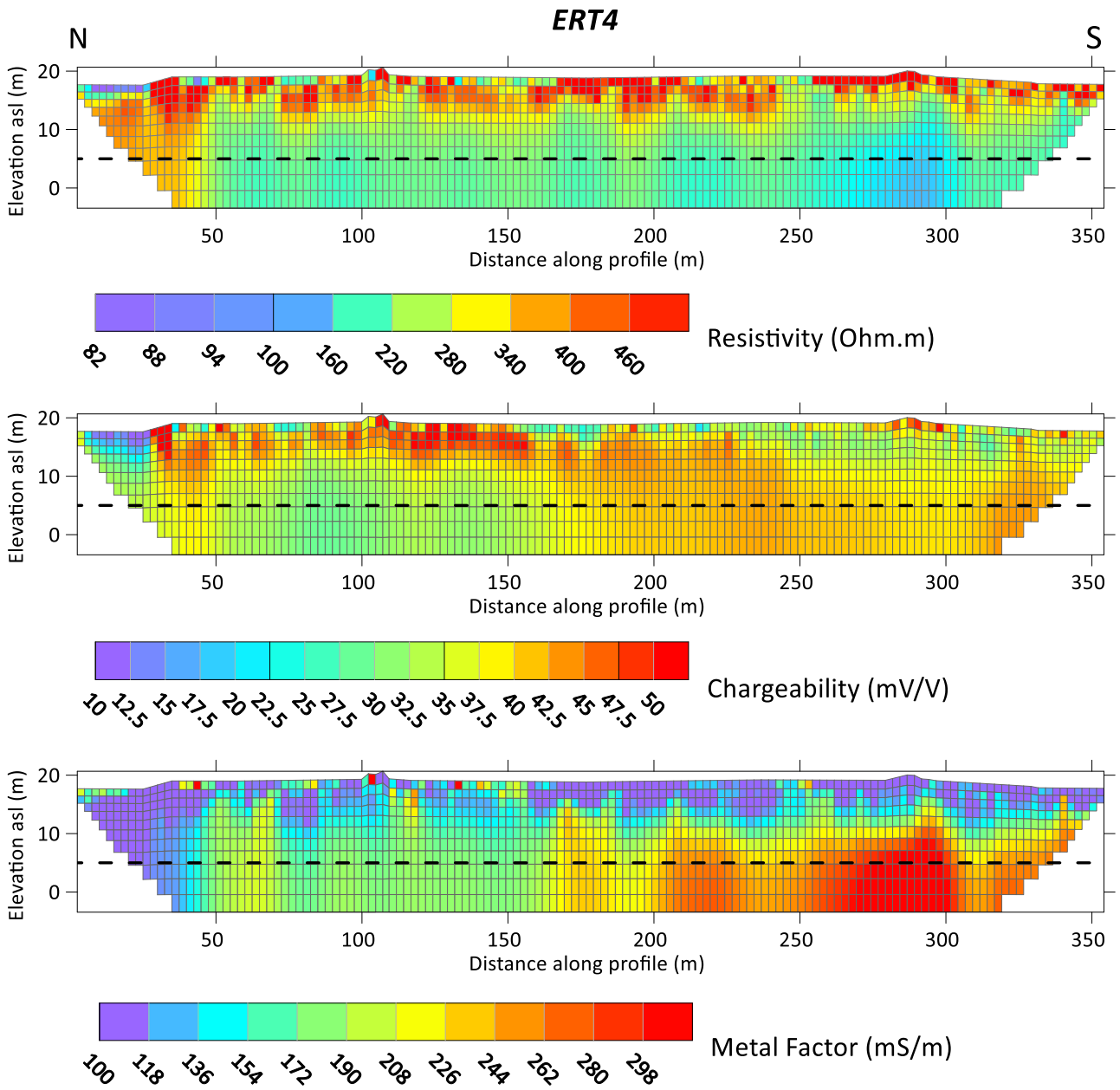


Figure 35 : ERT4.tomography. Top : Electrical resistivity cross-section, middle : Chargeability cross-section, bottom: Metal Factor cross-section. Dash black line represents the mean elevation of the heap bottom. Res2Inv inversion results.

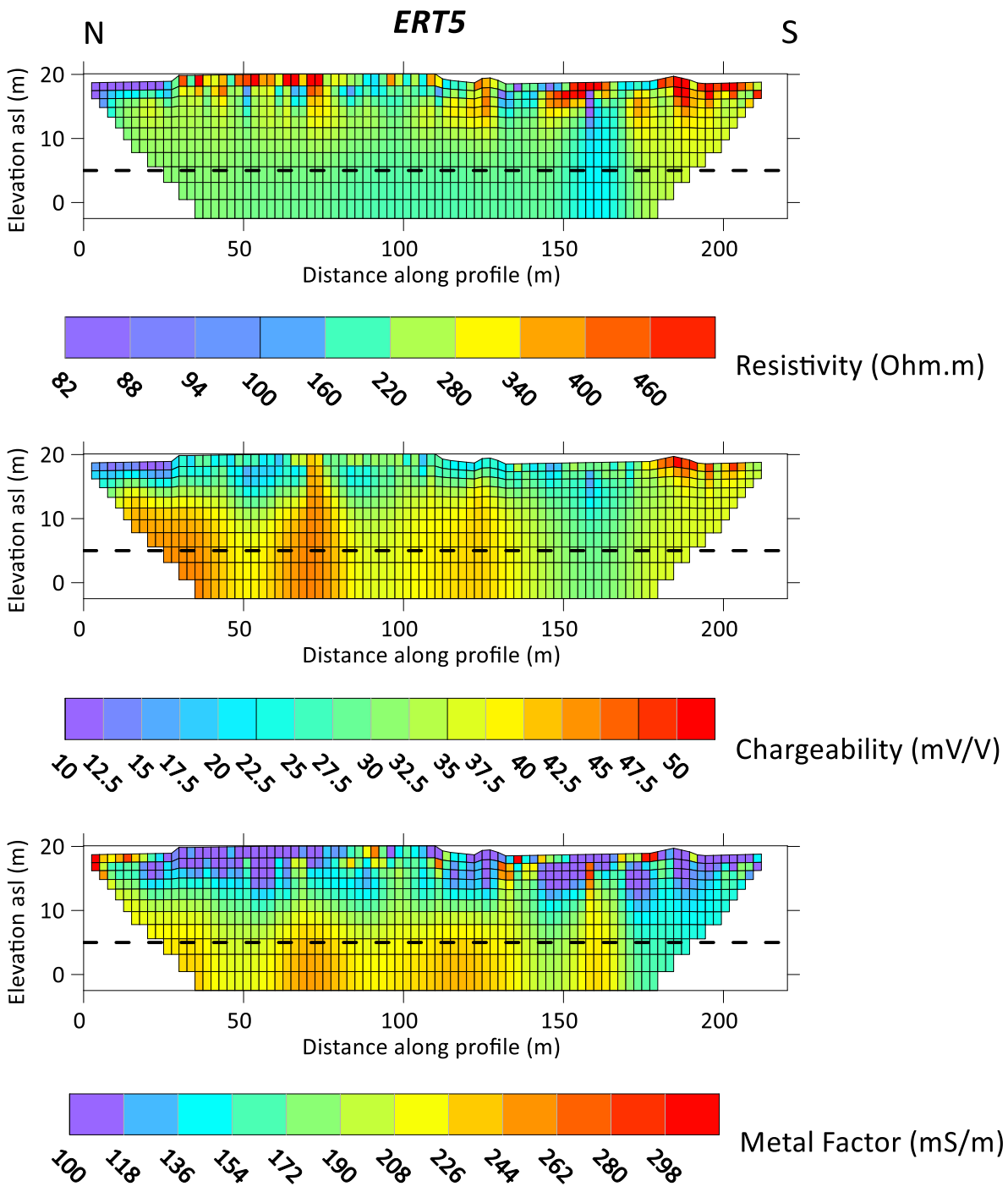


Figure 36 : ERT5.tomography. Top : Electrical resistivity cross-section, middle : Chargeability cross-section, bottom: Metal Factor cross-section. Dash black line represents the mean elevation of the heap bottom. Res2Inv inversion results.

3.3.3 ERT Results

On the five profiles, the limit between waste heap and the natural soil is not clear, whatever the geophysical parameter. However, natural layer below the wastes composed of sandy clayey marine sediments is more conductive from the elevation 5 m to -1 m asl, and is much more conductive below -1m asl, where salty intrusion could decrease the resistivity, especially on ERT1 profile where the depth of investigation is much higher than on the other profiles. At the opposite, waste materials are more resistive. In the North-West part of the heap, a conductive body is visible within the heap material, between abscise 80 and 120m on ERT1, and between abscise 75 and 200 m on ERT2. These materials have a moderate chargeability 10 to 20 mV/V, but a high metal factor (100 to 200 mS/m).

In any case, these resistivity, chargeability and metal factor cross-sections don't reveal waste structures or layering in the heap. These cross-sections show a patchy organization that confirms the large heterogeneity of wastes as was already demonstrated with the geomagnetic results.

The following description represents specific observations on each profile.

On profile ERT1 (Figure 32), a resistive, high chargeability layer waste material is visible between elevation 13 and 17m asl and abscise 0 to 120 m.

On profile ERT2 (Figure 32), a dipping high chargeability layer is visible between abscise 220 (top elevation 19m) and 350m (top elevation 9m). This layer has a moderate metal factor (250 to 300 mS/m) and the layer is no longer visible with this parameter. A horizontal high MF layer is visible between abscise 120 and 200 m (elevation 6 to 15 m asl).

On profile ERT3 (Figure 34), the only remarkable feature is a high chargeability (40 to 50 mV/V) and moderate MF (1500 to 200 mS/m) layer between abscise 100 and 300m, and elevation 14 and 17m asl).

The profile ERT4 (Figure 35) shows the same dipping high chargeability layer as on ERT2, as ERT4 and ERT2 are parallel and separated by 20 to 40 m. The dipping layer starts at the abscise 100 m and ends at the abscise 280 m (top layer from elevation 9 to 17 m asl). However, this layer has a moderate MF (between 200 and 250 mS/m).

The profile ERT5 (Figure 36) is situated on the eastern side of the heap. It does not show any remarkable feature. A moderate chargeability and moderate MF layer is visible at bottom of the heap between abscise 25 and 120 m.

4 SYNTHESIS AND DISCUSSION

4.1 SYNTHESIS OF RESULTS

The geomagnetic and EMI surveys show that the surficial magnetic susceptibility of slags is high and locally highly variable. As a consequence, the geomagnetic map and electrical conductivity maps are heterogeneous and no classification is possible based on geomagnetic and EMI data.

As electrical resistivity and IP tomography techniques are not sensitive to magnetic susceptibility, it is possible to classify the slag and other metallurgical wastes on Teesside site (CLE31) based on their resistivity and IP signatures. At least, 3 different types of slags have been identified. Using results from the 5 ERT profiles carried out on the slag heap, the geometry and the volume of these different kind of wastes can be calculated.

4.2 BOREHOLE LOCALIZATION

Considering the heterogeneous nature of the slag heap identified with the geophysical results, five (5) boreholes (Table 1 and Figure 37) are proposed to characterize each geophysical signature in terms of at least, metallic element concentrations (XRF), metallic particle identification (XDR), and granulometry.

Each borehole must reach the natural soil, i.e. their depth is approximately 13 to 15 m (see Figure 8)

Borehole B1 is located at the intersection of profiles ERT1 and ERT2. The purpose of B1 is to identify the origin of the conductive bottom layer in the central part.

Borehole B2 is located between ERT2 and ERT4, in the South of the site. The purpose of B2 is to characterize the dipping highly chargeable layer.

Borehole B3 is located at the intersection of 3 profiles: ERT1, ERT3 and ERT4. As this point is common to 3 profiles over 5, the characterization of the wastes will explain a large part of the waste origin, by extrapolation from this borehole.

Borehole B4 is located 10 m west from profile ERT5. It is situated in a high surficial magnetic susceptibility area and crosses a deep high chargeability at the bottom of the wastes heap.

Borehole B5 is located in the eastern part of profile ERT3. The purpose of B5 is the characterization of layers with changing chargeabilities and resistivities.

Table 1 : Table of coordinates of the 5 boreholes for control

UTM East (m)	UTM North (m)	Borehole label	Comments
622150	6053555	B1	Characterization of conductive layer in the central part
622102	6053407	B2	Characterization of dipping layer with high chargeability
622108	6053570	B3	Intersection between 3 profils : ERT1 –ERT 3- ERT4
622213	6053589	B4	Characterization of anomalies: <ul style="list-style-type: none"> - surficial high magnetic susceptibility - deep high chargeability
622150	6053471	B5	Characterization of dipping layer with high chargeability

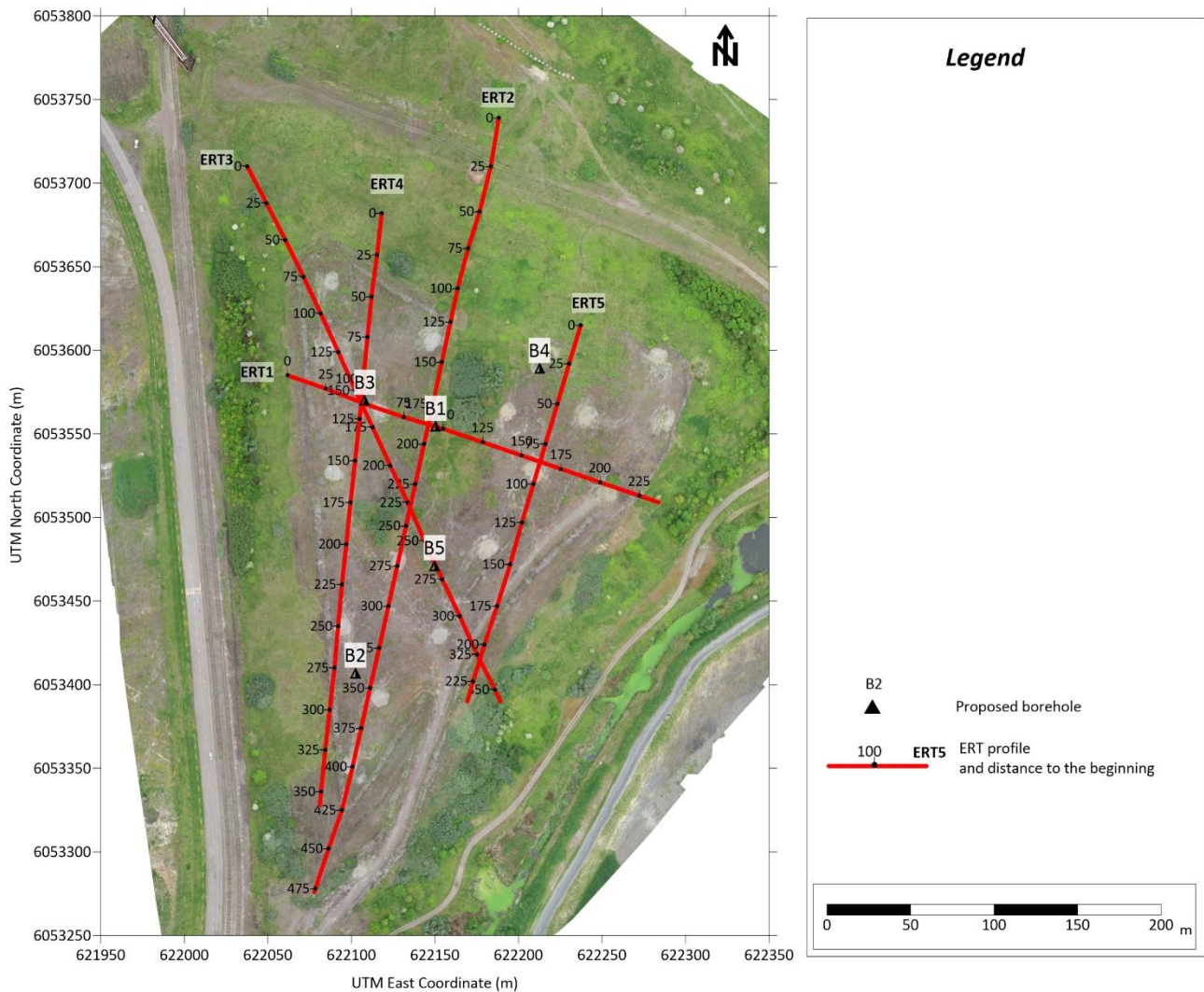


Figure 37 : Position of the 5 boreholes proposed for control

5 CONCLUSIONS

The geophysical survey carried out on the Teesside slag heap CLE31 show that the material filling the heap has variable and heterogeneous geophysical properties.

Magnetic and electromagnetic maps show randomly distributed parameters. The magnetic and electromagnetic surveys are affected by the local variations of magnetic susceptibility which is high and highly variable on these kind of wastes from iron metallurgy. Thus, magnetic and electromagnetic surveys are difficult to interpret in such context. Based on our observations on the Teesside site, these techniques are not recommended for mapping wastes from iron metallurgy, especially if they contain high level of magnetite. However, they highlighted the heterogeneous nature of the wastes that are likely to have been deposited randomly.

The electrical resistivity and IP tomography are not affected by highly magnetically susceptible materials. These techniques allow to distinguish one layer and several anomalies with homogeneous electrical properties within the heap. A dipping highly chargeable layer is located in middle of the heap on profiles ERT2 and ERT4. In the context of Teesside heap CLE31, ERT results show poor

layering and poor homogeneity within the heap. The slag heap was likely built from waste of very different origins.

Five boreholes are proposed and positioned with local specific geophysical signatures to study further the main anomalies observed with geophysical methods and go further towards a quantitative interpretation of the slag heap structure. Physico-chemical and metallic compounds analyses on cores are proposed to complete the dataset on the Teesside site investigations within the NWE-REGENERATIS project.

6 REFERENCES

Flores Orozco, A., Gallistl, J., Bucker, M., & Williams, K. H. (2018). Decay curve analysis for data error quantification in time-domain induced polarization imaging. *GEOPHYSICS*, 83(2), Art. 2. <https://doi.org/10.1190/geo2016-0714.1>

Günther, T., Rücker, C., & Spitzer, K. (2006). Three-dimensional modelling and inversion of dc resistivity data incorporating topography—II. Inversion. *Geophysical Journal International*, 166(2), 506- 517. <https://doi.org/10.1111/j.1365-246X.2006.03011.x>

Mc Neil J.D., 1980, Electromagnetic terrain conductivity measurement at low induction numbers, Technical Note TN-6, Geonics, Mississauga, Canada.

Rücker, C., Günther, T., & Wagner, F. M. (2017). pyGIMLi : An open-source library for modelling and inversion in geophysics. *Computers & Geosciences*, 109, 106- 123. <https://doi.org/10.1016/j.cageo.2017.07.011>

Slater, L., Binley, A. M., Daily, W., & Johnson, R. (2000). Cross-hole electrical imaging of a controlled saline tracer injection. *Journal of Applied Geophysics*, 44(2), Art. 2. [https://doi.org/10.1016/S0926-9851\(00\)00002-1](https://doi.org/10.1016/S0926-9851(00)00002-1)